energies

MDPI

Article

Evaluating the Risk of Exceeding the Normal Operating Conditions of a Low-Voltage Distribution Network due to Photovoltaic Generation

Roman Korab [1,*], Marcin Połomski [2] and Marcin Smołka [3]

[1] Department of Power Systems and Control, Faculty of Electrical Engineering, Silesian University of Technology, 44-100 Gliwice, Poland
[2] Department of Algorithmics and Software, Faculty of Automatic Control, Electronics and Computer Science, Silesian University of Technology, 44-100 Gliwice, Poland; marcin.polomski@polsl.pl
[3] TAURON Polska Energia S.A. and Joint Doctoral School, Silesian University of Technology, 44-100 Gliwice, Poland; marcin.smolka@polsl.pl
* Correspondence: roman.korab@polsl.pl

Abstract: Connecting photovoltaic micro-installations to a low-voltage network changes the operating conditions of the network. As a result, in certain situations, the permissible operating limits may be periodically exceeded. The risk of exceeding the normal operating conditions of the network depends on multiple factors, including the installed capacity of the photovoltaic sources. In this article, we use a time-series method to determine the annual risks of exceeding the bus voltage limits, the rated current of the lines and transformer, and the acceptable limit of the negative sequence component of bus voltage, as well as the risk of a reverse flow occurring, and the risk of energy losses increasing. We calculate these risks for different levels of penetration of the photovoltaic sources, different divisions of the rated power of the photovoltaic sources between individual phases, and different consumer load profiles. We perform calculations on a CIGRE test network using OpenDSS and statistical meteorological data for the Katowice (Poland) weather station. The results obtained indicate that connecting photovoltaic micro-installations to a low-voltage network has the greatest impact on the risk of reverse flow occurring and the risk of energy losses increasing. In addition, the risk of overvoltage and branch overload increases substantially. The method we present allows one to determine the value of the hosting capacity of a given low-voltage network, ensuring that the assumed risk of exceeding the normal operating conditions of the network is retained.

Keywords: photovoltaic micro-installation; prosumer; low-voltage network; grid impact; hosting capacity; risk evaluation; time-series method; OpenDSS

check for updates

Citation: Korab, R.; Połomski, M.; Smołka, M. Evaluating the Risk of Exceeding the Normal Operating Conditions of a Low-Voltage Distribution Network due to Photovoltaic Generation. *Energies* **2022**, *15*, 1969. https://doi.org/10.3390/en15061969

Academic Editor: Albert Smalcerz and Marcin Blachnik

Received: 8 February 2022
Accepted: 7 March 2022
Published: 8 March 2022

Publisher's Note: MDPI stays neutral with regard to jurisdictional claims in published maps and institutional affiliations.

Copyright: © 2022 by the authors. Licensee MDPI, Basel, Switzerland. This article is an open access article distributed under the terms and conditions of the Creative Commons Attribution (CC BY) license (https://creativecommons.org/licenses/by/4.0/).

1. Introduction

Solar energy has developed rapidly in recent years, with photovoltaic (PV) power generation one of its most prominent applications. Worldwide, in 2020, cumulative installed PV capacity exceeded 707 GW and represented 25% of the total installed capacity of renewable energy sources [1]. Within many regions globally, including European countries that are subject to moderate insolation, PV power generation is exhibiting rapid growth. In Poland, PV sources are the fastest-growing power generation technology, with a total installed rated power of 3.94 GW at the end of 2020, increasing from 1.47 GW the previous year (an increase of 170%) [2]. More than 75% of the installed capacity of PV sources in Poland comes from micro-installations.

According to Polish distribution system operators [3], in mid-2021, there were over 600,000 micro-installations connected to the grid (on-grid), and the average rated power of the newly connected installation was 7.64 kW. Development of PV micro-installations in Poland has surged throughout 2019–2020; at the end of 2018, only 54,000 PV sources were

connected to the grid. Such an increase has been caused by the implementation of support mechanisms for prosumers: individuals who both produce and consume energy. These support mechanisms include investment subsidies [4] and a favorable settlement scheme for the energy produced [5]. Due to the planned continuation of these mechanisms, we assume that the upward trend in the number of grid-connected PV micro-installations will continue.

On-grid micro-installations are connected to a low-voltage (LV) network. On average, prosumers for their current needs consume approximately 30% of the energy they produce [6]; as a consequence, there are periods during the day when generation exceeds demand. If, as in the majority of cases, the prosumer does not possess a suitable form of energy storage, the excess of generated energy is transmitted to the grid. If there are relatively few prosumers within a given area, the energy generated by micro-installations is negligible, and the operation of the grid is unaffected. However, if there are many prosumers, the total power generated by photovoltaic installations can be large enough to produce periodic adverse effects on the operation of the LV network. These adverse effects primarily include the following:

- A voltage rise, leading to overvoltage [7–12];
- An increase in voltage unbalance [11,12];
- An increase in current flow, leading to the overload of network components [7,10];
- The appearance of reverse power flows; for example, power flows from the LV grid to the medium voltage (MV) grid [9,12]; and
- Increased power losses [8,9,12].

Photovoltaic sources connected to the LV grid also increase voltage fluctuations and affect the level of harmonics, the value of short-circuit currents, and the rotor angle stability.

To safely integrate PV sources into an LV network, the impact of these sources on the network must be analyzed. The maximum amount of distributed energy resources (DER) that a given distribution network can accommodate without exceeding its normal operating conditions and without requiring infrastructure development is known as the hosting capacity (HC) [13–16]. Generally, HC is mainly limited by:

- Overvoltage—power generation that is greater than load can cause the bus voltage to exceed acceptable levels and potentially damage devices connected to the bus [13,15,16];
- Voltage unbalance—the unequal loading of phases increases the negative sequence component of voltage, thereby decreasing the power quality [16];
- Thermal overload—lines and transformers can overheat if their rated currents are exceeded, leading to various operational failures [15,16];
- Protection problems—the reverse power flow caused by DER generation can lead to the unintentional activation of protective systems during normal conditions, or the malfunction of such systems during fault conditions [13,15]; and
- Power losses—DER generation can decrease the transmission efficiency of the distribution network, leading to an increase in energy losses [15].

There is no unique HC for a given LV network. The HC depends directly on the selection and quantification of the limiting factors. The HC also depends on the size of the individual PV micro-installations and their location within the network. However, the most important factor affecting the HC is the risk of exceeding the operational limits that distribution network operators and customers are willing to accept [17].

Traditionally, stochastic methods are used to assess risk in power systems [18]. Such methods have been used recently to determine the risk of disturbances within grids with connected PV sources [19–24]. Stochastic methods are suitable due to the stochastic variability of PV generation, which is caused by the unpredictability of weather conditions leading to variable solar irradiance. Other unknown variables include customer load, the size and location of PV sources, and the availability of network components. These uncertainties are included in stochastic methods by the use of probability distribution functions. The state of the analyzed power grid is then determined by sampling the assumed probability

distribution functions of each variable. Once the grid states are obtained, the power flow can be calculated for each state. Statistical methods are used to illustrate the results.

One drawback of stochastic methods is their considerable computational complexity; as the number of unknown variables increases, so does the complexity and run time of the simulation. However, the most notable shortfall of such methods is the mutual independence of the system variables over time. Where the relationship between systems variables is important, time-series methods are required.

Time-series methods [14] take power consumption and PV production time series' as inputs. This approach accounts for correlations between different uncertain parameters such as load and solar irradiance. The input data can be taken from direct measurements or can be generated using appropriate stochastic process models. By combining the data with a distribution grid model, output profiles can be obtained via power flow calculations.

The use of time-series methods allows uncertainties to be handled appropriately. These methods provide a realistic overview of the operation of the grid under different levels of PV penetration, accounting for the time-varying nature of power consumption and generation. As in the case of stochastic methods, computational complexity is an important consideration also in time-series methods. The computation time is a function of the time resolution and length of the time series. Typical time resolutions are 10 min, 15 min, and one hour, and the typical length of a time series can range from one year to several years [14]. The choice of resolution and length of the time series depends on data availability.

In the article, we use a time-series method to determine the risk of exceeding the normal operating conditions of an LV distribution network due to PV generation. We use a three-phase low-voltage network model with four time series' as inputs: power consumption, solar irradiance, wind speed, and ambient temperature. Each time series has a time resolution of one hour and a length of one year. Bus voltages, branch currents, and energy losses are calculated for each hour of the year analyzed. Using this approach, we determine the number of hours in the year for which the following hold:

- The voltage of a given bus is higher than 1.1 V_{n} or lower than 0.9 V_{n}, where V_{n} is the nominal voltage of the network;
- The negative sequence component of voltage in a given bus is greater than 2% of the positive sequence component;
- The current flow in a given network component (line or transformer) is greater than the rated current of that device;
- The reverse power flow from the LV grid to the MV grid appears;
- The energy losses within the LV grid are greater when PV sources are connected than without PV sources.

By determining these values, we can calculate the risk of exceeding the normal operating conditions of the LV distribution grid due to PV generation. For the given time series' and the location of the PV micro-installations within the network, the level of risk depends on the rated power of the connected sources; the greater the total power of the PV sources, the greater the risk. Therefore, the HC can be set in accordance with the level of risk accepted by the distribution system operator and customers.

The remainder of this article is organized as follows. Section 2 provides a detailed description of the CIGRE test network, the simulation environment, the input data, and the proposed risk calculation method. Section 3 presents the results obtained from the time-series method for different penetration levels of the PV sources, different divisions of the rated power of the PV sources between individual phases, and different consumer load profiles. Section 4 discusses the results, and Section 5 presents the conclusions and suggests future work.

2. Materials and Methods

2.1. Test Network and Simulation Environment

The CIGRE technical brochure [25] provides models of test systems in various configurations, which can be used to analyze the influence of DER on the operation of power

systems. The LV test network we selected from the brochure, shown in Figure 1, is a three-phase cable network that supplies residential consumers. The network has a conventional European configuration (TN-C). Figure 1 also shows the peak powers of complex loads representing groups of customers supplied by individual buses. The given values apply to three-phase loads and are divided proportionally between the three phases (complex loads are star connected with the neutral wire).

MV equivalent network:

Nominal voltage = 20 kV

Short circuit power = 100 MVA

X/R ratio = 1

Transformer:

Rated power = 500 kVA

Nominal voltage ratio = 20 kV/ 0.4 kV

Short circuit voltage = 4.12%

Load losses = 1%

Connection = 3-phases Dyn

Underground cables:

C1: Al, 240 mm²

C2: Al, 50 mm²

Line length:

L1: 30 m

L2: 35 m

□ – cable joint

LV network type: TN-C

Grounding resistances:

Transformer: R = 3 Ω

Network (PEN): R = 40 Ω

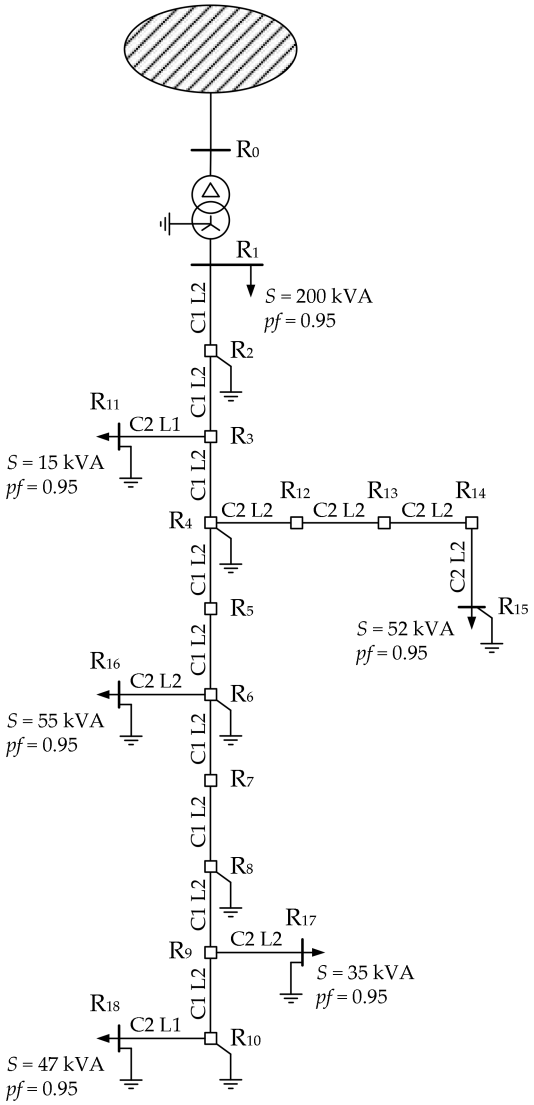

Figure 1. Diagram of the CIGRE LV test network for supplying residential consumers, showing component parameters.

We simulated the LV test network using the open-source electric power distribution system simulator OpenDSS, developed by the Electric Power Research Institute [26]. OpenDSS is designed to support DER grid integration and power network modernization. It provides support for the complex analysis of current and future power networks, using configurable models of individual grid components. Notably, OpenDSS is capable of calculating power flows in multiphase power system networks with the inclusion of asymmetric loads and power generation.

2.2. Yearly Load Variability

The load values shown in Figure 1 demonstrate the peak load of the CIGRE test network. The technical brochure [25] also provides the daily load profile of the customers, shown in Figure 2. This profile is the same for all loads.

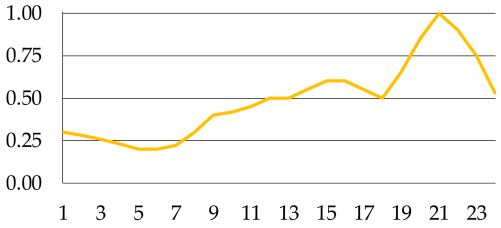

Figure 2. The daily load profile (p.u. of peak load) of residential loads in the CIGRE test network.

We prepared yearly load profiles for each customer using the daily load profile. Each time series had a time resolution of one hour and a length of one year. We used two types of yearly load profiles: symmetric and asymmetric. To generate the symmetric profiles, we treated each daily load profile throughout the year as identical and consistent with the profile shown in Figure 2 for each phase and all customers. As an example, Figure 3 shows the weekly symmetric load profile. In contrast, the yearly asymmetric load profiles were generated randomly around the symmetric profile, which was used as a mean. To create the random profiles, we used a pseudorandom number generator with a normal distribution. The coefficient of variation (the ratio of standard deviation to mean) was assumed to be a constant of 0.3 for each customer throughout the simulation period. We replaced any negative load values that were sampled with the corresponding value from the symmetric load profile. Figure 4 shows the weekly asymmetric load profile. The total energy consumed during the year by all customers connected to the CIGRE network was 1644.7 MWh for the symmetric load profile and 1646.1 MWh for the asymmetric profile.

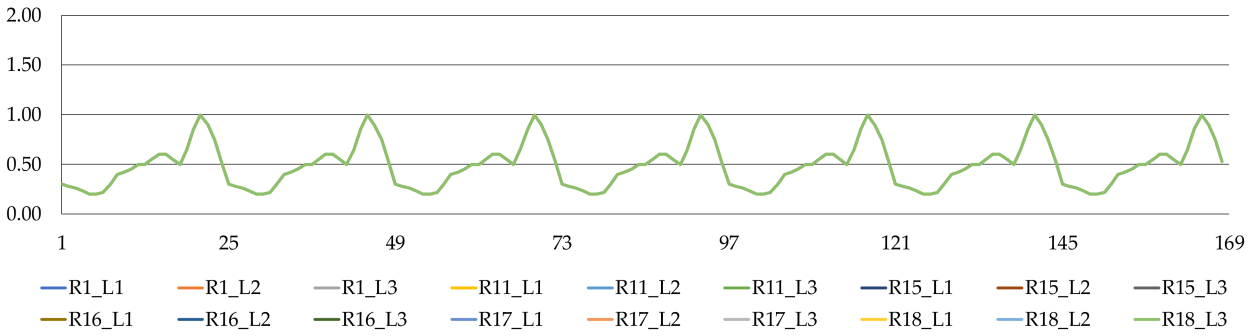

Figure 3. Weekly symmetric load profile (p.u. of peak load).

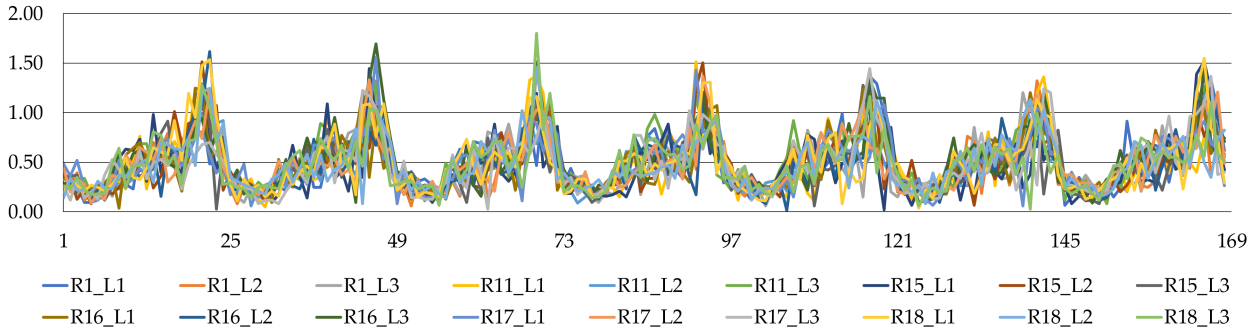

Figure 4. Weekly asymmetric load profile (p.u. of peak load).

2.3. Determination of PV Penetration Level and the Rated Power of Individual PV Sources

The literature lacks consensus on the definition of PV penetration level [16,27]. A possible definition is the ratio of the total rated power of all PV sources to the peak load of the network or the rated capacity of the transformer. Another definition is the ratio of customers with PV generators to the total number of customers in the given area. The PV penetration level (PL) can also be defined based on energy consumption, as the ratio of the total yearly energy generated by the PV systems (E_{PV}) to the total yearly energy (E) consumed by customers connected to the analyzed network:

$$PL = \frac{E_{PV}}{E} \times 100\%. \quad (1)$$

In the article, we use the last definition. For the simulations, we assumed two PV penetration levels (PL = 25% and PL = 50%) corresponding with two levels of yearly energy generated by the PV sources within the test network: E_{PV} = 1644.7 MWh × 0.25 = 411.2 MWh for PL = 25%, and E_{PV} = 1644.7 MWh × 0.5 = 822.4 MWh for PL = 50%.

From the E_{PV} value, it is possible to determine the rated power of the PV sources. When calculating this power, the billing method for the energy produced by the prosumer should be considered. Poland has no fixed tariff for the surplus energy generated by prosumers. Instead, prosumers can exchange the surplus energy for energy received from the grid. If the PV source is rated at 10 kW or lower, for every 1 kWh of energy supplied to the grid, the prosumer can receive 0.8 kWh in return without any charge, with the settlement being made on an annual basis. As such, prosumers treat the power system as virtual energy storage with an efficiency of 0.8. The above rules can be encapsulated in a formula to calculate P_{rPV}, the required rated power of a PV installation:

$$P_{rPV} = SC\frac{E_{PV}}{CF \times 8760} + (1 - SC)\frac{\frac{E_{PV}}{EVS}}{CF \times 8760}, \quad (2)$$

where the self-consumption coefficient SC is the yearly energy generated by the PV source that is consumed immediately by the customer, the PV capacity factor CF is the ratio of the actual yearly production to the maximum possible yearly production, EVS is the efficiency of virtual energy storage, and 8760 (with units of hours) is the number of hours in a year.

We assume that the PV sources are connected to each load bus of the CIGRE test network and that the PV penetration level is the same for each bus. We used the following values to calculate the rated power of the PV sources: CF = 0.114, a typical value for Poland; SC = 0.25; and EVS = 0.8. We assumed that the rated power of a PV source connected to a given bus is the sum of the rated power of multiple micro-installations, each with a capacity of no more than 10 kW. Table 1 shows the rated power of the PV sources calculated using Formula (2) for the two PV penetration levels.

Table 1. Rated power of PV sources for two PV penetration levels.

Load Bus					PL = 25%		PL = 50%	
No	**S**	**pf**	**P**	**E**	E_{PV}	P_{rPV}	E_{PV}	P_{rPV}
-	kVA	-	kW	MWh	MWh	kW	MWh	kW
R_1	200	0.95	190.0	814.2	203.6	241.7	407.1	483.4
R_{11}	15	0.95	14.3	61.1	15.3	18.1	30.6	36.3
R_{15}	52	0.95	49.4	211.7	52.9	62.8	105.8	125.7
R_{16}	55	0.95	52.3	223.9	56.0	66.5	111.9	132.9
R_{17}	35	0.95	33.3	142.5	35.6	42.3	71.2	84.6
R_{18}	47	0.95	44.7	191.3	47.8	56.8	95.7	113.6
Sum	404	-	384.0	1644.7	411.2	488.2	822.4	976.5

The rated power of the PV sources applies to three-phase installations. Within the simulations, the powers of installations are divided symmetrically and asymmetrically between the three phases. The asymmetrical division was generated randomly and is different for each load bus but the same for both PV penetration levels. The division of the rated power of the PV sources between the individual phases of the load buses is shown in Figure 5. The yearly energy generated by the PV sources during simulation does not differ by more than 0.1% from the assumed energy used to calculate the rated power of the sources.

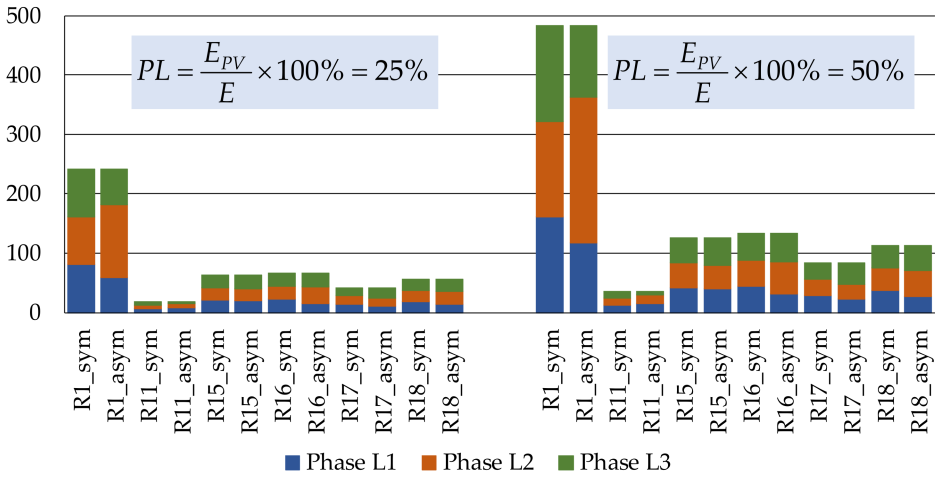

Figure 5. Division of the rated power of PV sources (kW) between the individual phases of the load buses in the CIGRE test network.

2.4. Model of a PV Source

The PV source model used by OpenDSS is presented in Figure 6. To parameterize the model, we first define the rated power of the PV panels P_{rPV} under standard test conditions. The power generated by the PV panels is determined for a given level of solar irradiance and is dependent upon the panel temperature, so the obtained power value must be corrected accordingly. The temperature of the PV panels T_{PV} is calculated using an external model based on the ambient temperature T_a, solar irradiance intensity SI, and wind speed WS [28]:

$$T_{PV} = T_a + SI \times e^{-3.473 - 0.0594 \times WS}. \quad (3)$$

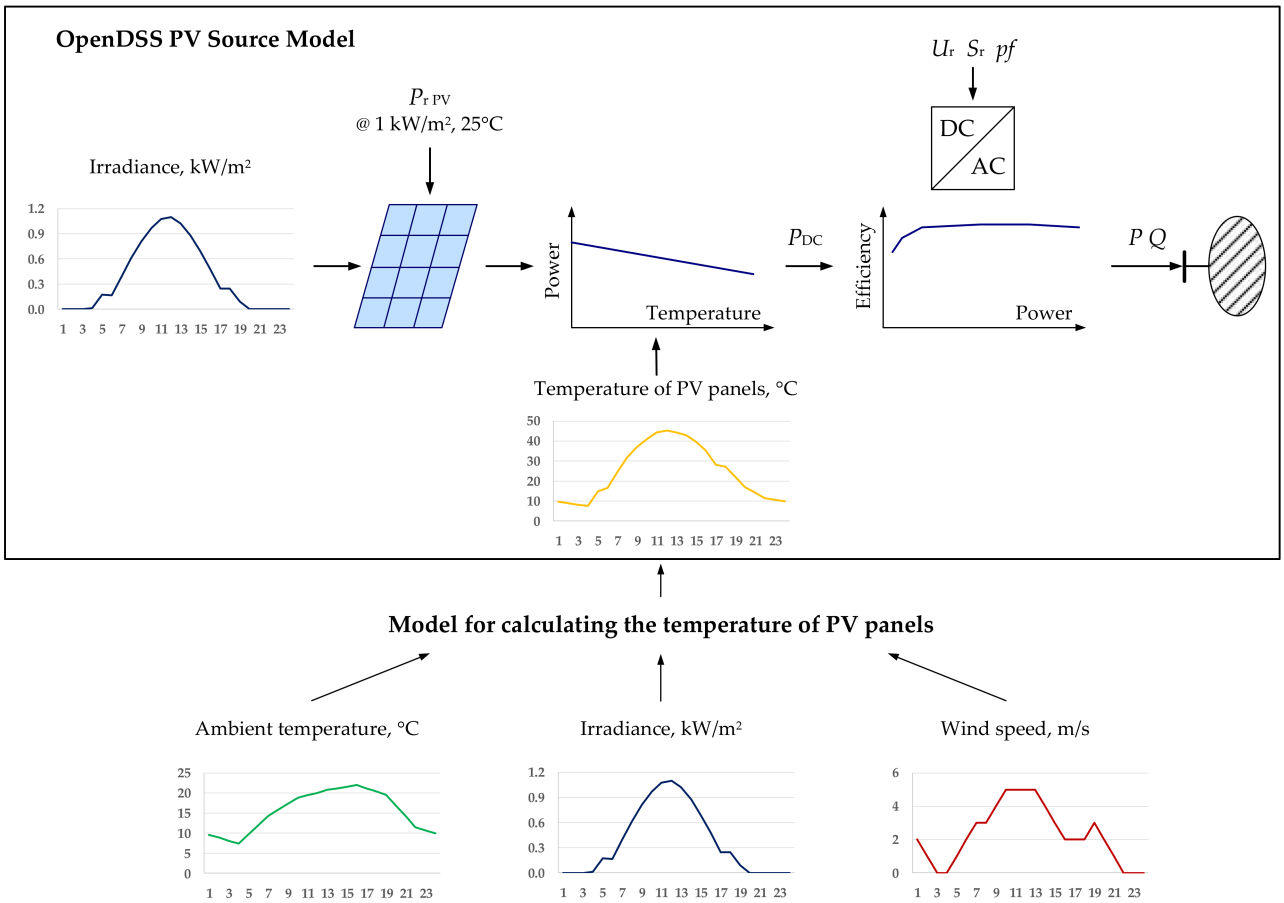

Figure 6. The PV source model used by OpenDSS, with the daily profiles of ambient temperature, solar irradiance, and wind speed based on the weather conditions on 17 May.

The DC power generated P_{DC} is then converted according to the efficiency characteristic of the inverter, for which the rated power S_r, rated voltage U_r, and power factor pf are given. The active power P and the reactive power Q generated by the PV source are calculated at the output of the inverter.

2.5. The Variability of Weather Conditions

As described in the previous section, PV electricity generation is dependent upon solar irradiance and other atmospheric variables that affect panel efficiency. Therefore, PV performance is predominantly influenced by the variables that define the weather conditions for a particular day and location. As such, to calculate the power generation of PV sources, we require meteorological data. The data we used corresponded to typical meteorological years, sets of data that have been prepared to fulfill the needs of energy calculations, energy auditing, design works, and simulations. The methodology to prepare a typical meteorological year was developed by the International Organization for Standardization and accepted by the Comité Européen de Normalisation as the EN ISO 15927–4:2005 standard [29]. The 12 months of weather data are selected from at least 10 years of meteorological observations for a given location. Figures 7–10 present, respectively, ambient temperature, wind speed, solar irradiance, and calculated PV panel surface temperature during a typical meteorological year, obtained by the Katowice meteorological station, located at 50°14′ N 19°02′ E [30].

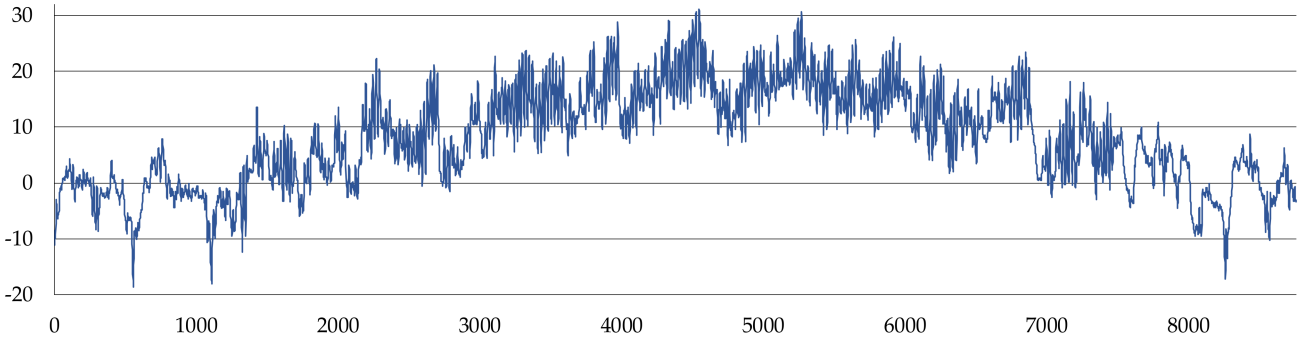

Figure 7. Ambient temperature (°C) during the typical meteorological year for the Katowice meteorological station.

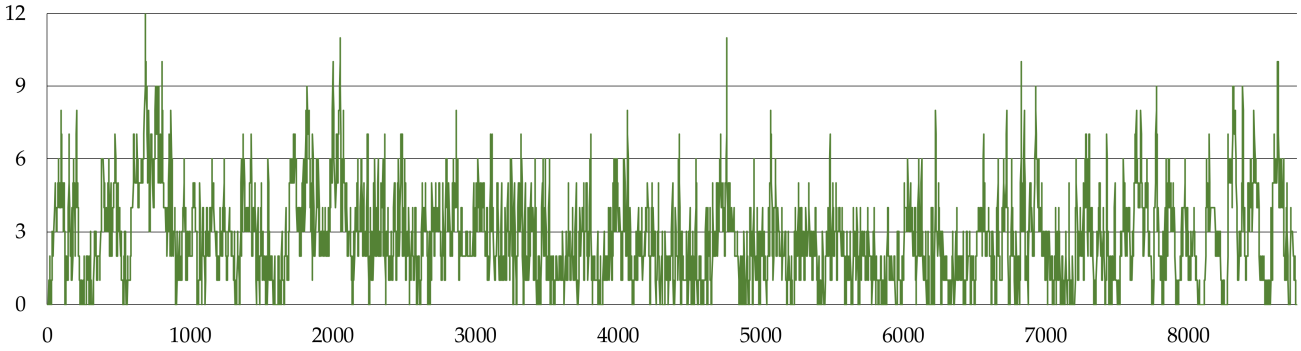

Figure 8. Wind speed (m/s) during the typical meteorological year for the Katowice meteorological station.

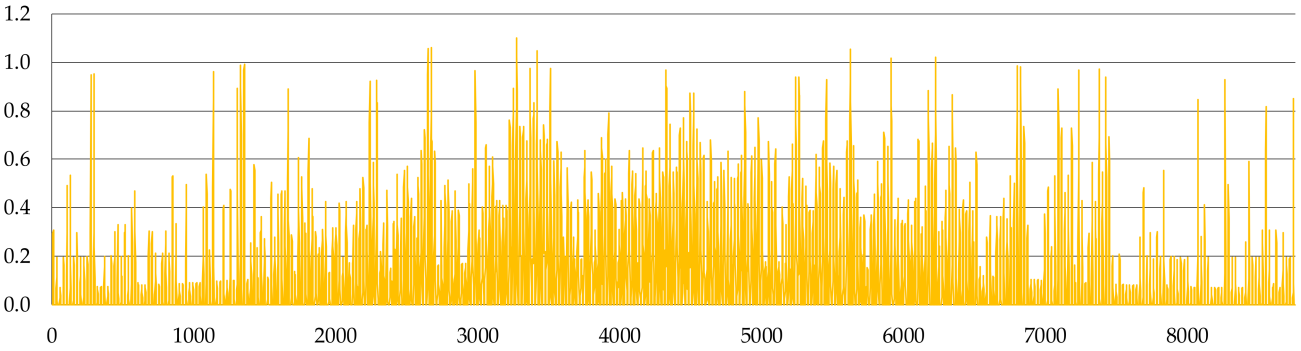

Figure 9. Solar irradiance (kW/m^2) during the typical meteorological year for the Katowice meteorological station.

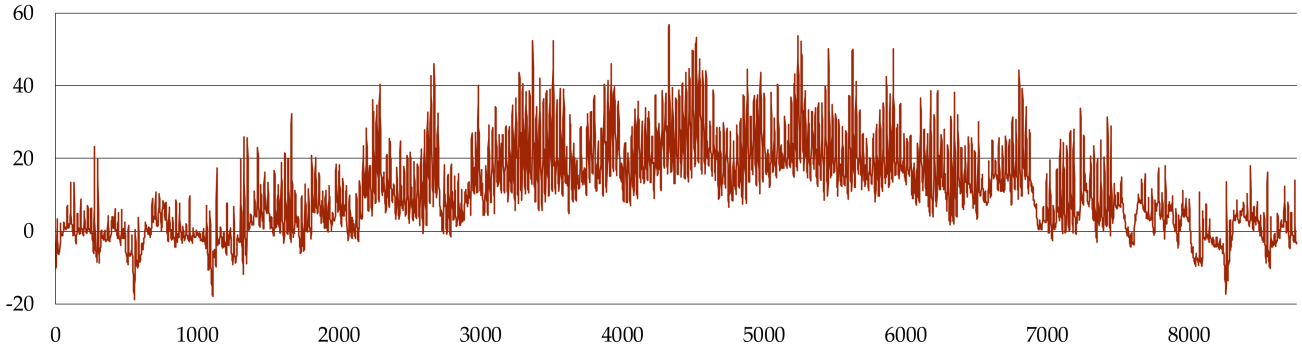

Figure 10. PV panel surface temperature (°C) during the typical meteorological year calculated on the basis of the ambient temperature, solar irradiance intensity, and wind speed for the Katowice meteorological station.

2.6. Variants of the CIGRE Test Network Operating Conditions

Using the load profiles defined in Section 2.2, in addition to the PV penetration levels and the division of the rated power of the PV sources between individual phases, defined in Section 2.3, we defined ten variants of operating conditions for the test network simulations. The defined variants are shown in Table 2. The simulations for each variant used the same weather conditions described in Section 2.5.

Table 2. The ten variants of operating conditions used in yearly simulations of the CIGRE test network.

		V1	V2	V3	V4	V5	V6	V7	V8	V9	V10
Load profile	Symmetric	x	x	x	x	x					
	Asymmetric						x	x	x	x	x
PV penetration level	0%	x					x				
	25%		x		x			x		x	
	50%			x		x			x		x
Division of the PV-rated power	Symmetric		x	x				x	x		
	Asymmetric				x	x				x	x

2.7. Risk Calculation

To assess the risk of exceeding the normal operating conditions of the LV network due to PV generation, we first define normal operating conditions for the network:

- The voltage of each bus is within the range 0.9–1.1 V_n [31];
- The negative sequence component of voltage in each bus is not greater than 2% of the positive sequence component [31];
- The current flow within each branch does not exceed the rated current of the transformer and cable lines; for the test network, the transformer is rated for 722 A, and we assume that the rated current of the cable lines is 401 A for a cross-section of 240 mm^2 and 157 A for a cross-section of 50 mm^2 [32];
- The reverse power flow, i.e., the power flow from LV to MV network, does not appear;
- Energy losses do not exceed those incurred without PV sources.

Severity degrees are commonly used to calculate the risks associated with the operation of PV sources in power systems [19,20,22,23]. We also use this concept in the article. We define several severity degrees as follows. The severity degrees of the upper and lower limits of bus voltage are given by:

$$S_{\overline{V}} = \begin{cases} V_i - V_{\max} & \text{if} \quad V_i > V_{\max} \\ 0 & \text{if} \quad V_i \leq V_{\max} \end{cases}, \tag{4}$$

$$S_V = \begin{cases} V_{\min} - V_i & \text{if} \quad V_i < V_{\min} \\ 0 & \text{if} \quad V_i \geq V_{\min} \end{cases}, \tag{5}$$

where V_i is the voltage at bus i, and $V_{\max}$ and $V_{\min}$ are the upper and lower limits of the voltage, respectively. The severity degree of the upper limit of the negative sequence component of the bus voltage is given by:

$$S_{V2} = \begin{cases} \left(\frac{V_{2i}}{V_{1i}} \times 100\% - 2\%\right) & \text{if} \quad \frac{V_{2i}}{V_{1i}} \times 100\% > 2\% \\ 0 & \text{if} \quad \frac{V_{2i}}{V_{1i}} \times 100\% \leq 2\% \end{cases}, \tag{6}$$

where V_{1i} and V_{2i} are the positive sequence and negative sequence components of the voltage at bus i, respectively. The severity degree of the rated current of a branch is given by:

$$S_I = \begin{cases} I_i - I_r & \text{if} \quad I_i > I_r \\ 0 & \text{if} \quad I_i \leq I_r \end{cases}, \tag{7}$$

where I_i is the current flow in branch i, and I_r is the rated current of the branch. The severity degree of the reverse power flow is given by:

$$S_R = \begin{cases} I_{LV \to MV} & \text{if} \quad I_{LV \to MV} > 0 \\ 0 & \text{if} \quad I_{LV \to MV} \leq 0 \end{cases}, \tag{8}$$

where $I_{LV \to MV}$ is the current flow from the LV network to the MV network. The severity degree of energy losses is given by:

$$S_{\Delta E} = \begin{cases} \Delta E_{PV} - \Delta E & \text{if} \quad \Delta E_{PV} > \Delta E \\ 0 & \text{if} \quad E_{PV} \leq \Delta E \end{cases}, \tag{9}$$

where ΔE_{PV} and ΔE are the energy losses in the entire network with and without PV sources, respectively.

Based on the simulation results, we calculated the severity degrees defined by Formulas (4)–(9) for each hour of the analyzed year. We then determined the number of hours during the year when each severity degree is greater than zero. On this basis, the risk of exceeding the normal operating conditions of the network is given by:

$$R_{S_i} = \frac{N_{S_i>0}}{N} \cdot 100\%, \tag{10}$$

where $i = (\overline{V}, V, V2, \text{I}, \text{R}, \Delta\text{E})$, $N_{S_i>0}$ is the number of hours during the year when the value of the i-th severity degree is greater than zero, and $N = 8760$ is the total number of hours in a year. We calculated $S_{\overline{V}}$, S_V, S_I, and S_R for the individual phase-to-phase voltages and phase currents, while S_{V2} and $S_{\Delta E}$ for individual buses or the entire network, respectively. We calculated the risk values in the same manner.

3. Results

3.1. Results of the Daily Simulations for Symmetric Load Profile without PV Sources—Variant V1

Tables 3 and 4 show the calculated voltages and currents within the CIGRE test network under the peak load condition shown in Figure 1. We found that the results obtained using OpenDSS were consistent with those presented in the CIGRE brochure [25], confirming the correct implementation of the test network in OpenDSS. The observed unbalance of voltages and currents for individual phases of a given bus or branch results from the impedance unbalance of the network (for the calculations, we assumed a phase symmetry of loads).

Table 3. Phase-to-phase voltages (V) for load buses in the CIGRE test network.

Bus	Phases	CIGRE	O_DSS	Bus	Phases	CIGRE	O_DSS
	L1–L2	393.04	393.04		L1–L2	375.84	375.86
R_1	L2–L3	393.02	393.02	R_{16}	L2–L3	377.58	377.60
	L3–L1	393.01	393.02		L3–L1	376.21	376.23
	L1–L2	385.83	385.84		L1–L2	373.40	373.42
R_{11}	L2–L3	386.61	386.62	R_{17}	L2–L3	375.56	375.59
	L3–L1	385.98	385.99		L3–L1	373.86	373.88
	L1–L2	370.02	370.03		L1–L2	372.32	372.35
R_{15}	L2–L3	371.49	371.50	R_{18}	L2–L3	374.59	374.61
	L3–L1	370.33	370.34		L3–L1	372.81	372.84

Table 4. Current flows (A) in branches that supply load buses in the CIGRE test network.

Branch	Phase	CIGRE	O_DSS	Branch	Phase	CIGRE	O_DSS
	L1	557.69	557.72		L1	74.28	74.29
R_0–R_1	L2	559.38	559.18	R_6–R_{16}	L2	74.73	74.68
	L3	561.07	561.28		L3	75.18	75.24
	L1	20.84	20.85		L1	46.91	46.92
R_3–R_{11}	L2	20.90	20.89	R_9–R_{17}	L2	47.27	47.23
	L3	20.96	20.96		L3	47.63	47.67
	L1	69.19	69.19		L1	62.80	62.81
R_{14}–R_{15}	L2	69.55	69.51	R_{10}–R_{18}	L2	63.30	63.24
	L3	69.88	69.93		L3	63.81	63.86

Respectively, Figures 11 and 12 illustrate the daily variability of phase-to-phase voltages in load buses and the daily variability of current flows in the branches that supply those buses. The variability is the result of the assumed load profile shown in Figure 2. For variant V1, this variability is identical for each day of the year. The results presented in Figures 11 and 12 constitute a background for the analysis of the impact of PV sources on the operating conditions of the CIGRE test network.

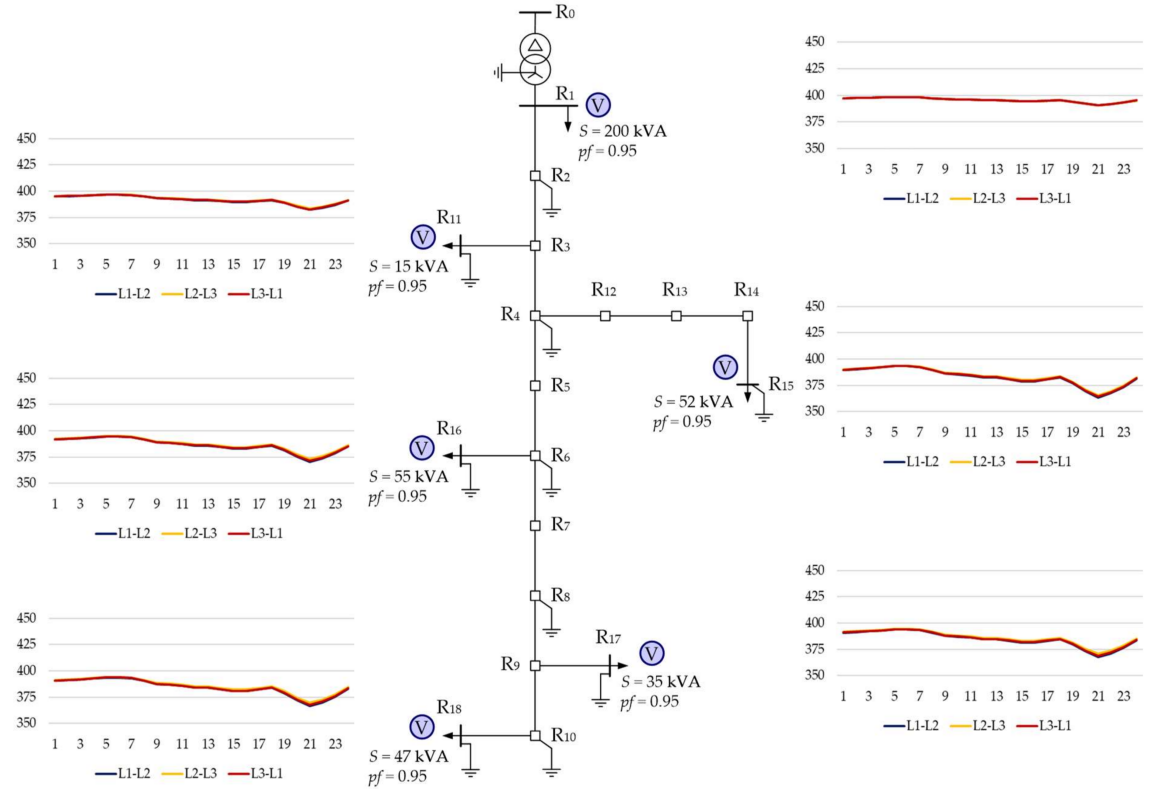

Figure 11. Daily simulation results showing the phase-to-phase voltages (V) in the test network for variant V1.

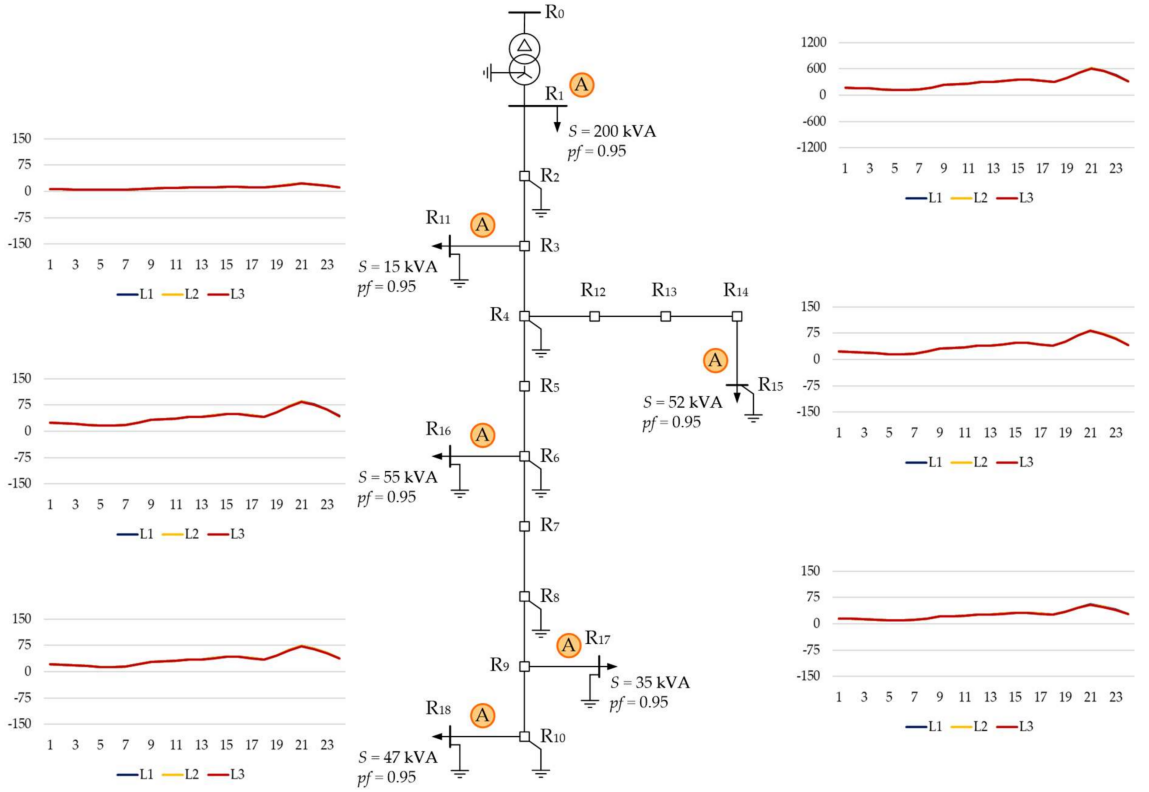

Figure 12. Daily simulation results showing the phase currents (A) in the test network for variant V1.

3.2. Results of the Daily Simulations for the Symmetric Load Profile with Symmetric PV Sources—Variants V2 and V3

The PV source models, with the rated power given in Table 1, were implemented in the CIGRE test network model. For each model, yearly simulations of network operation were performed for the weather conditions described in Section 2.5. We present the simulation results for 17 May, the day on which the maximum intensity of solar irradiance was observed; the weather conditions for 17 May are shown in Figure 6.

Figure 13 compares the total load and the total PV generation in the CIGRE test network for the two PV penetration levels. The results show that for both variants, there are periods during the day when the generation of PV sources exceeds the load. It is during these hours that the largest changes in network operation conditions should be expected. This is illustrated by Figures 14–17, which show the daily voltage and current profiles in the test network when the PV sources are connected.

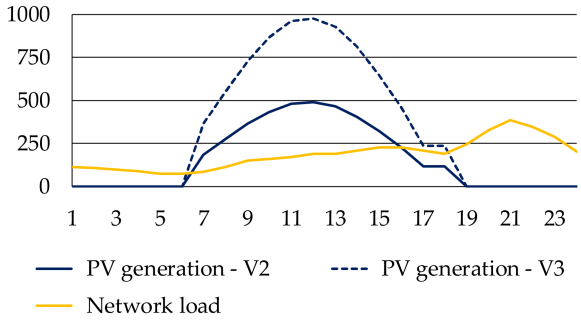

Figure 13. Total daily load and total PV generation (kW) in the CIGRE test network.

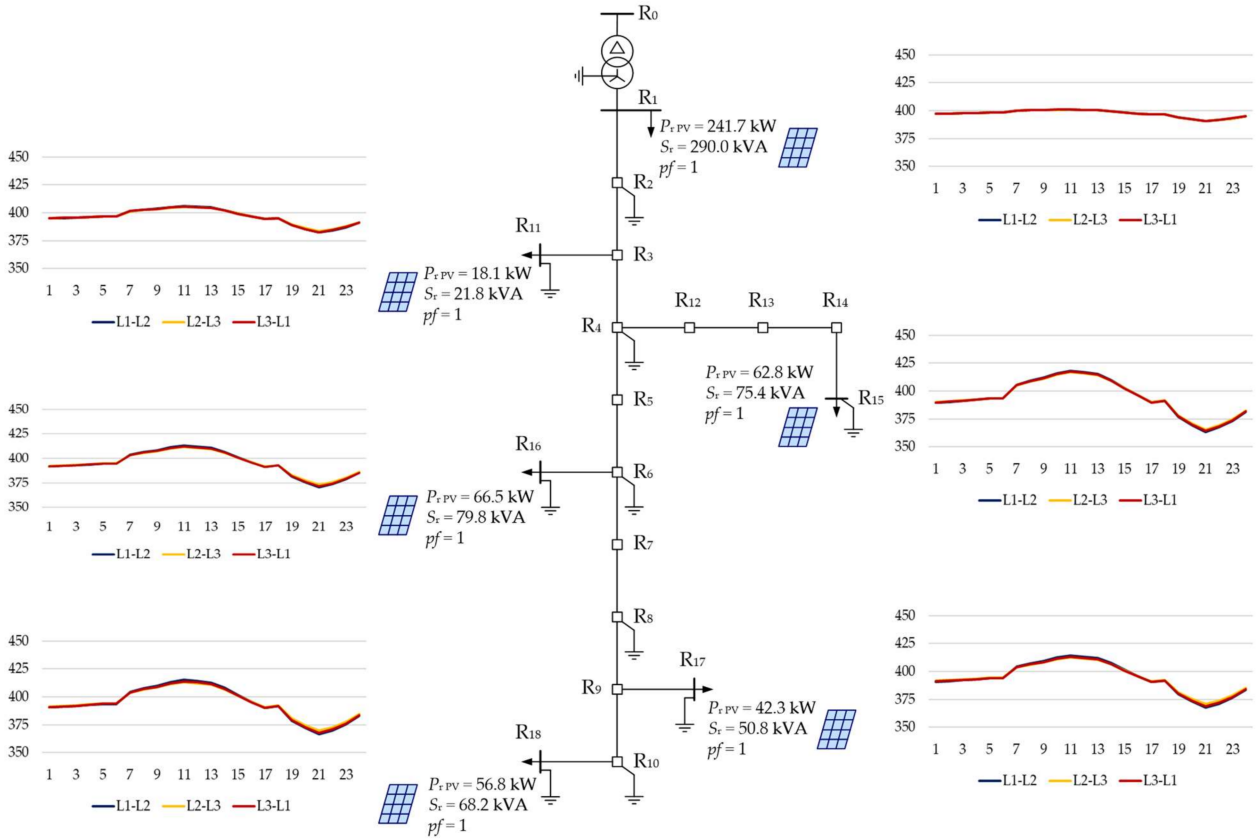

Figure 14. Daily simulation results showing the phase-to-phase voltages (V) in the test network for variant V2.

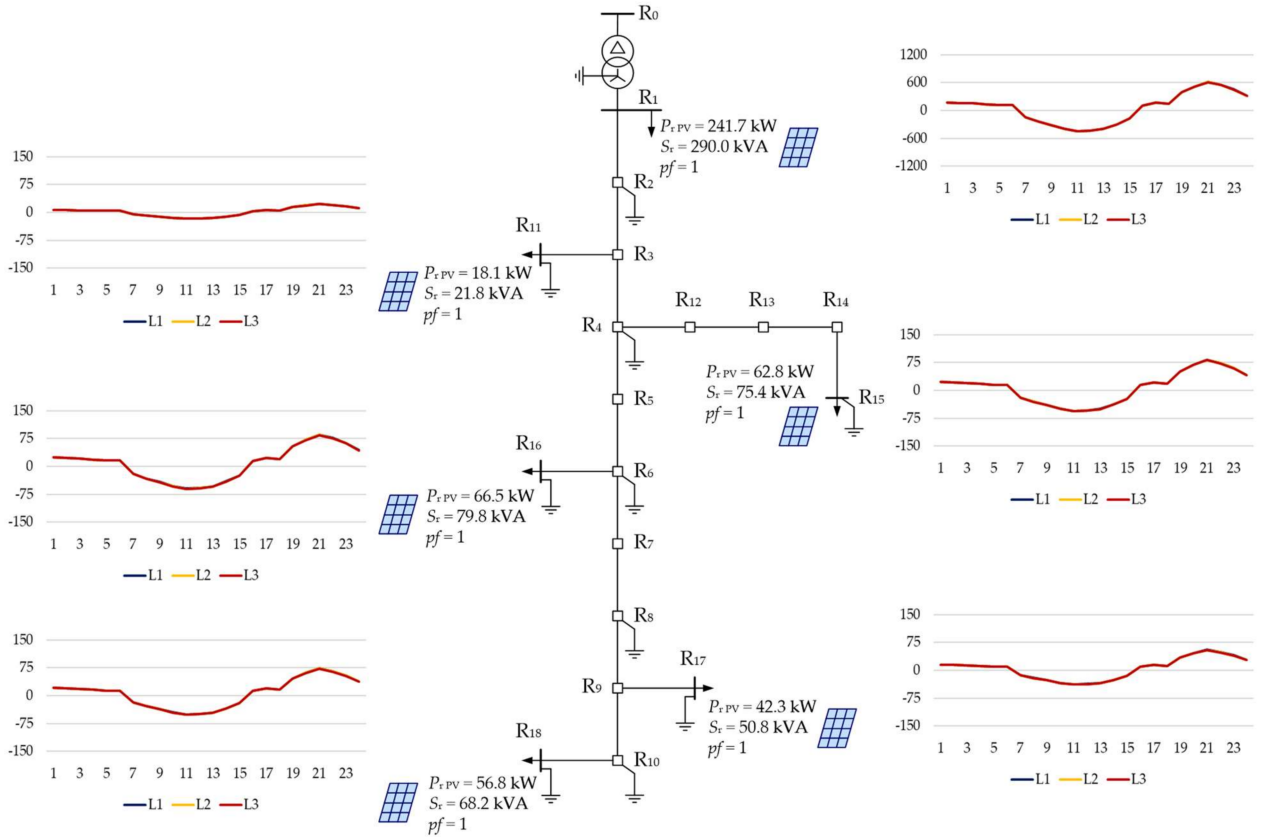

Figure 15. Daily simulation results showing the phase currents (A) in the test network for variant V2.

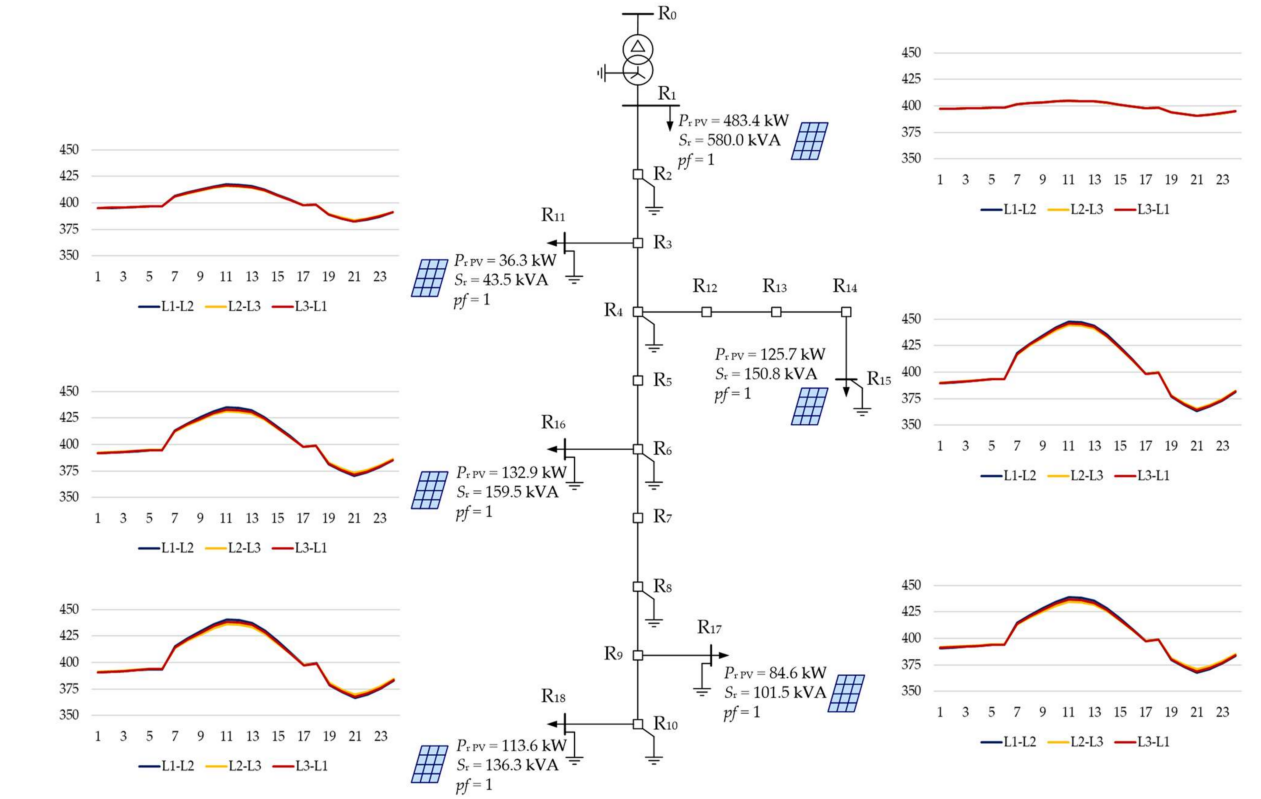

Figure 16. Daily simulation results showing the phase-to-phase voltages (V) in the test network for variant V3.

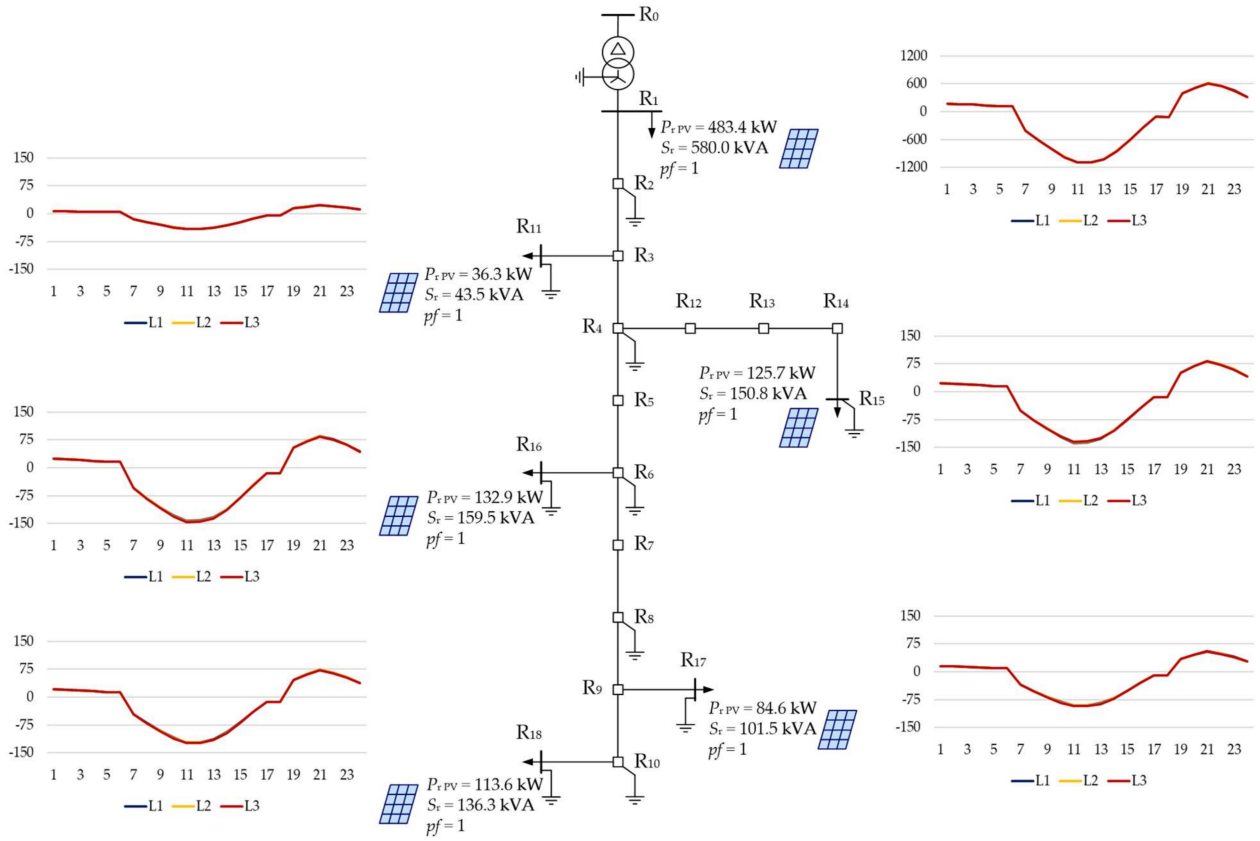

Figure 17. Daily simulation results showing the phase currents (A) in the test network for variant V3.

Power generation via PV sources also affects the negative sequence component of the bus voltage and the transmission losses. Figures 18 and 19 show a comparison of these parameters for variants V1, V2, and V3. Appendix A presents the simulation results for the remaining operating condition variants.

3.3. Results of the Yearly Simulations—Values of Risk of Exceeding the Normal Operating Conditions of the CIGRE Test Network

As a result of the yearly simulations, the values of bus voltages, branch currents, symmetrical components, and network losses were calculated for each hour during the year for every variant of the CIGRE test network operating conditions. From this, we calculated the severity degrees defined by Formulas (4)–(9) and the corresponding risk values defined by Formula (10). The results are presented in Tables 5–10.

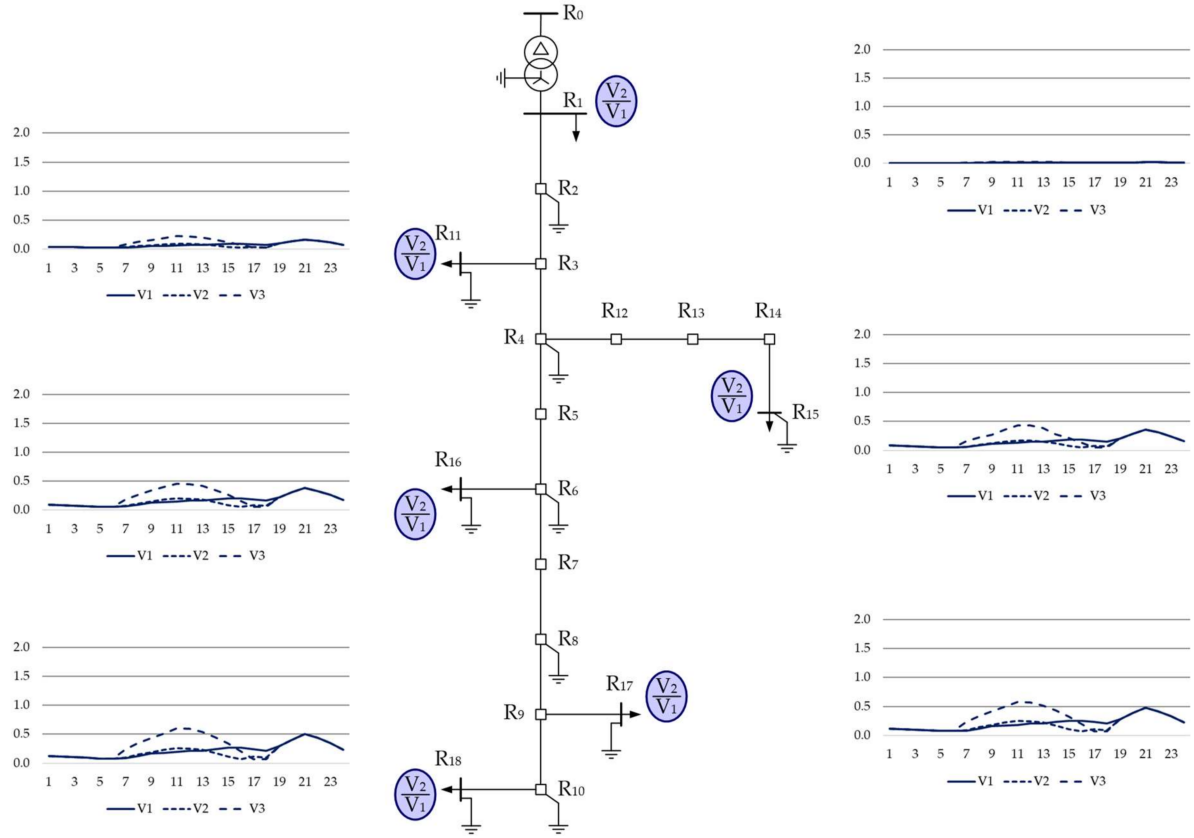

Figure 18. Daily simulation results showing the negative sequence component of the bus voltage (%) for variants V1, V2, and V3.

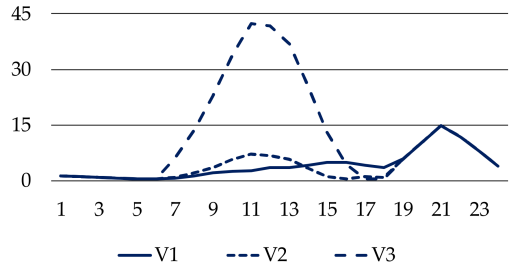

Figure 19. Daily simulation results showing the energy losses (kWh) for variants V1, V2, and V3.

Table 5. The risk of exceeding the upper limit of the bus voltage $R_{S_{\overline{V}}}$ (%) for load buses in the CIGRE test network.

Bus	Phases	Variants of the CIGRE Test Network Operating Conditions									
		V1	**V2**	**V3**	**V4**	**V5**	**V6**	**V7**	**V8**	**V9**	**V10**
R_1	L1–L2	0	0	0	0	0	0	0	0	0	0
	L2–L3	0	0	0	0	0	0	0	0	0	0
	L3–L1	0	0	0	0	0	0	0	0	0	0
R_{11}	L1–L2	0	0	0	0	0	0	0	0	0	0
	L2–L3	0	0	0	0	0	0	0	0	0	0
	L3–L1	0	0	0	0	0	0	0	0	0	0
R_{15}	L1–L2	0	0	0.51	0	0.01	0	0	0.48	0	0
	L2–L3	0	0	0.26	0	0.76	0	0	0.26	0	0
	L3–L1	0	0	0.35	0	0.55	0	0	0.40	0	0
R_{16}	L1–L2	0	0	0	0	0	0	0	0	0	0
	L2–L3	0	0	0	0	0.01	0	0	0	0	0.03
	L3–L1	0	0	0	0	0	0	0	0	0	0
R_{17}	L1–L2	0	0	0	0	0	0	0	0.01	0	0
	L2–L3	0	0	0	0	0.19	0	0	0	0	0.15
	L3–L1	0	0	0	0	0	0	0	0	0	0
R_{18}	L1–L2	0	0	0.03	0	0	0	0	0.03	0	0
	L2–L3	0	0	0	0	0.34	0	0	0	0	0.33
	L3–L1	0	0	0	0	0	0	0	0	0	0.01

Table 6. The risk of dropping below the lower limit of the bus voltage R_{S_V} (%) for load buses in the CIGRE test network.

Bus	Phases	Variants of the CIGRE Test Network Operating Conditions									
		V1	**V2**	**V3**	**V4**	**V5**	**V6**	**V7**	**V8**	**V9**	**V10**
R_1	L1–L2	0	0	0	0	0	0	0	0	0	0
	L2–L3	0	0	0	0	0	0	0	0	0	0
	L3–L1	0	0	0	0	0	0	0	0	0	0
R_{11}	L1–L2	0	0	0	0	0	0	0	0	0	0
	L2–L3	0	0	0	0	0	0	0	0	0	0
	L3–L1	0	0	0	0	0	0	0	0	0	0
R_{15}	L1–L2	0	0	0	0	0	1.87	1.87	1.87	1.87	1.87
	L2–L3	0	0	0	0	0	1.26	1.26	1.26	1.26	1.26
	L3–L1	0	0	0	0	0	0.74	0.74	0.74	0.74	0.74
R_{16}	L1–L2	0	0	0	0	0	0.03	0.03	0.03	0.03	0.03
	L2–L3	0	0	0	0	0	0.02	0.02	0.02	0.02	0.02
	L3–L1	0	0	0	0	0	0	0	0	0	0
R_{17}	L1–L2	0	0	0	0	0	0.25	0.25	0.25	0.25	0.25
	L2–L3	0	0	0	0	0	0.11	0.11	0.11	0.11	0.11
	L3–L1	0	0	0	0	0	0.02	0.02	0.02	0.02	0.02
R_{18}	L1–L2	0	0	0	0	0	0.71	0.71	0.71	0.71	0.71
	L2–L3	0	0	0	0	0	0.24	0.24	0.24	0.24	0.24
	L3–L1	0	0	0	0	0	0.07	0.07	0.07	0.07	0.07

Table 7. The risk of exceeding the upper limit of the negative sequence component of the bus voltage $R_{S_{V2}}$ (%) for load buses in the CIGRE test network.

Bus	Variants of the CIGRE Test Network Operating Conditions									
	V1	**V2**	**V3**	**V4**	**V5**	**V6**	**V7**	**V8**	**V9**	**V10**
R_1	0	0	0	0	0	0	0	0	0	0
R_{11}	0	0	0	0	0	0	0	0	0	0
R_{15}	0	0	0	0	0	0.40	0.40	0.40	0.40	0.40
R_{16}	0	0	0	0	0	0.01	0.01	0.01	0.01	0.01
R_{17}	0	0	0	0	0	0.03	0.03	0.03	0.03	0.03
R_{18}	0	0	0	0	0	0.06	0.06	0.06	0.06	0.06

Table 8. The risk of exceeding the rated current of branch R_{S_I} (%) in the CIGRE test network.

Branch	Phase	Variants of the CIGRE Test Network Operating Conditions									
		V1	**V2**	**V3**	**V4**	**V5**	**V6**	**V7**	**V8**	**V9**	**V10**
R_0–R_1	L1	0	0	1.44	0	0.34	0.67	0.67	2.15	0.67	1.00
	L2	0	0	1.50	0	4.57	0.72	0.72	2.16	0.72	5.43
	L3	0	0	1.51	0	0.96	0.76	0.76	2.35	0.76	1.78
R_1–R_2	L1	0	0	0.87	0	0.25	0.13	0.13	1.05	0.13	0.33
	L2	0	0	0.90	0	1.18	0.15	0.15	1.07	0.15	1.31
	L3	0	0	0.96	0	1.40	0.15	0.15	1.10	0.15	1.55
R_3–R_{13}	L1	0	0	0	0	0	0	0	0	0	0
	L2	0	0	0	0	0	0	0	0	0	0
	L3	0	0	0	0	0	0	0	0	0	0
R_{14}–R_{15}	L1	0	0	0	0	0	0	0	0	0	0
	L2	0	0	0	0	0	0	0	0	0	0
	L3	0	0	0	0	0	0	0	0	0	0
R_6–R_{16}	L1	0	0	0	0	0	0.02	0.02	0.02	0.02	0.02
	L2	0	0	0	0	0.33	0.01	0.01	0.01	0.01	0.38
	L3	0	0	0	0	0	0	0	0	0	0.03
R_9–R_{17}	L1	0	0	0	0	0	0	0	0	0	0
	L2	0	0	0	0	0	0	0	0	0	0
	L3	0	0	0	0	0	0	0	0	0	0
R_{10}–R_{18}	L1	0	0	0	0	0	0	0	0	0	0
	L2	0	0	0	0	0	0	0	0	0	0.02
	L3	0	0	0	0	0	0	0	0	0	0

Table 9. The risk of reverse power flow occurring R_{S_R} (%) in the CIGRE test network.

Branch	Phase	Variants of the CIGRE Test Network Operating Conditions									
		V1	**V2**	**V3**	**V4**	**V5**	**V6**	**V7**	**V8**	**V9**	**V10**
R_0–R_1	L1	0	13.50	21.99	9.20	20.07	0	13.68	21.66	9.50	20.00
	L2	0	13.50	22.00	17.83	22.47	0	13.66	21.70	17.57	22.42
	L3	0	13.50	22.00	12.03	21.26	0	13.72	21.84	12.17	21.29

Table 10. The risk of energy losses increasing $R_{\Delta E}$ (%) in the CIGRE test network.

Branch	Variants of the CIGRE Test Network Operating Conditions									
	V1	**V2**	**V3**	**V4**	**V5**	**V6**	**V7**	**V8**	**V9**	**V10**
Entire network	0	1.62	12.92	1.95	13.93	0	1.69	12.81	2.17	13.76

The results in Table 5 show that the voltage exceeded the upper limit in several load buses for variants V3, V5, V8, and V10, variants for which the penetration level of PV

sources is 50%. The highest risk was observed for bus R15. Figure 20 shows the number of hours during a year when the upper limit of bus R15 was exceeded. The degree by which it was exceeded is shown, in the ranges 0–1 V, 1–2 V, 2–3 V, etc. The data show that the upper limit of bus R15 is rarely exceeded by 5 V or more.

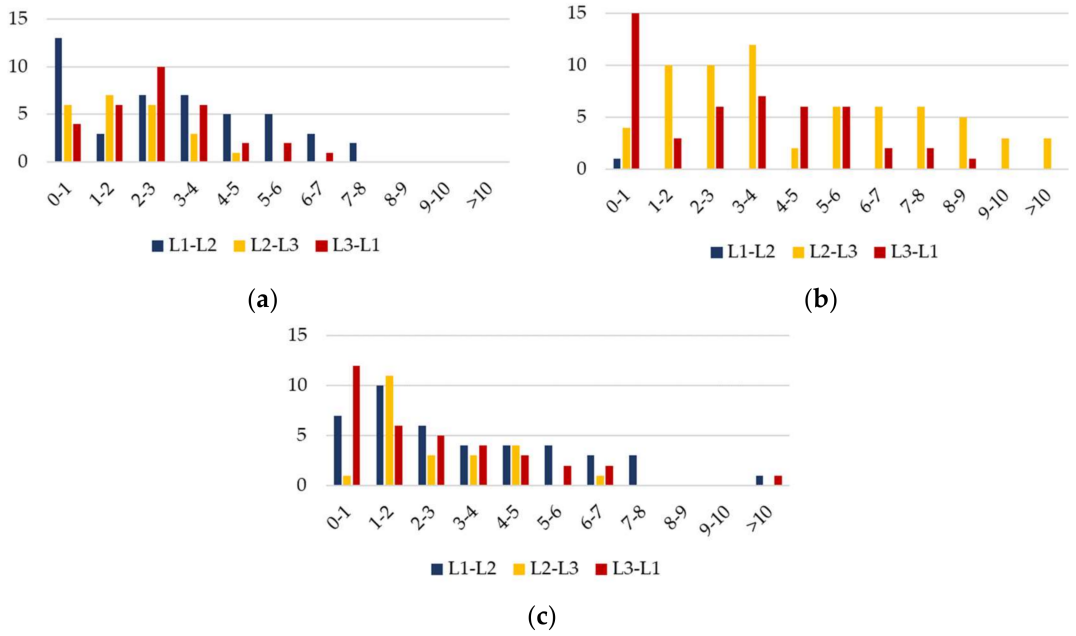

Figure 20. The number of hours in the year when the upper limit of the R15 bus voltage is exceeded within one of the defined ranges (V): (**a**) V3, (**b**) V5, and (**c**) V8.

Table 6 shows the risks that the load bus voltages drop below their minimum limits. The risks are non-zero for four buses when using variants V6–V10. The V1 and V6 variants have no PV sources. These variants differ only in the load profile; V1 has a symmetric load profile, while V6 has an asymmetric load profile. Hence, the voltage fell below the lower limit in the V6 variant due to an asymmetric load profile. The risks of the subsequent variants are the same as those of the V6 variant, indicating that for these variants, the PV sources did not increase the risk of dropping below the minimum limits of the bus voltages. A similar situation occurs in the case of the negative sequence component of the voltage, with the results shown in Table 7.

Table 8 shows the risks of exceeding the rated branch currents. The rated currents of the transformer (branch R_0–R_1) and lines R_1–R_2 are exceeded. The rated current of line R_2–R_3 is also exceeded; this is not shown in the table because the line operates in series with line R_1–R_2. The transformer and line-rated currents are exceeded when using variants V3, V5, V8, and V10, where the penetration level of PV sources is 50%. The rated currents of those components are also exceeded when using variants V6, V7, and V9; however, this is caused by the asymmetric load profile and not by the operation of the PV sources. When comparing variants V3 with V5 and V8 with V10, the asymmetric division of the PV-rated power noticeably impacts the load of the network branch. This impact can be favorable by mitigating overload, or unfavorable, by increasing overload. This issue is illustrated in Figure 21. Comparing Figure 21a–d shows that with the asymmetric division of the PV-rated power, the total number of hours in which the transformer overloads in phases L1 and L3 decreases, while the total number of hours in which the transformer overloads in phase L2 increases.

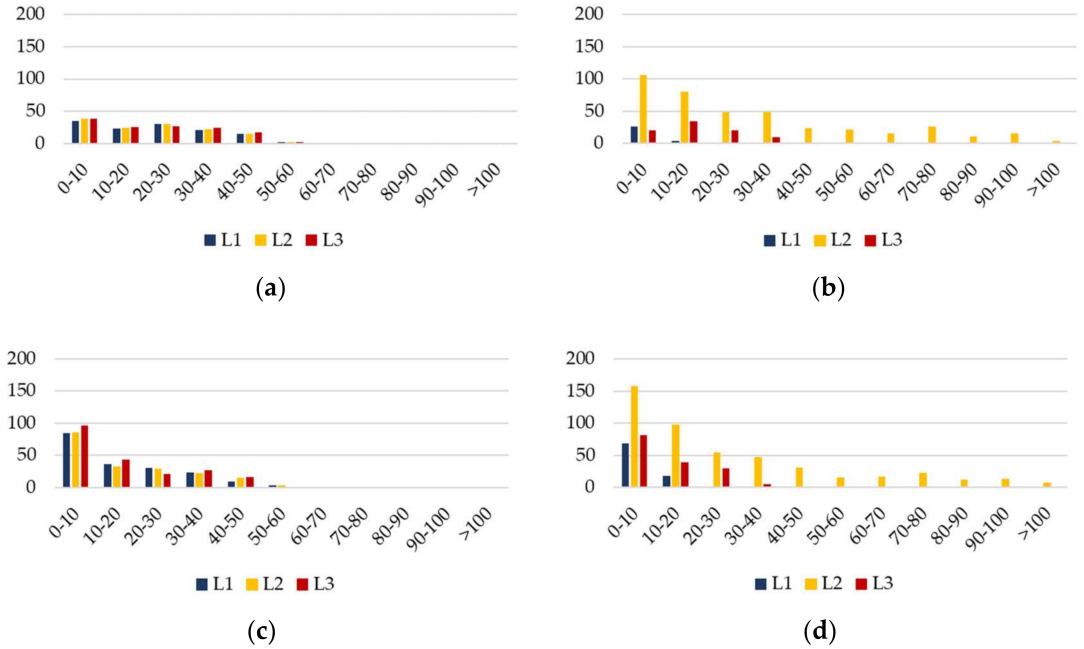

Figure 21. The number of hours during the year in which the rated current of the transformer (branch R_0–R_1) is exceeded by a value within the defined ranges (% of the rated current): (**a**) V3, (**b**) V5, (**c**) V8, and (**d**) V10.

In our simulations, reverse power flow occurred in each variant that contained PV sources. However, the risk of reverse flow is much higher in variants V3, V5, V8, and V10, where the penetration level of PV sources is 50% (see Table 9). The results show how the division of the PV-rated power between individual phases impacts the risk (Figure 22).

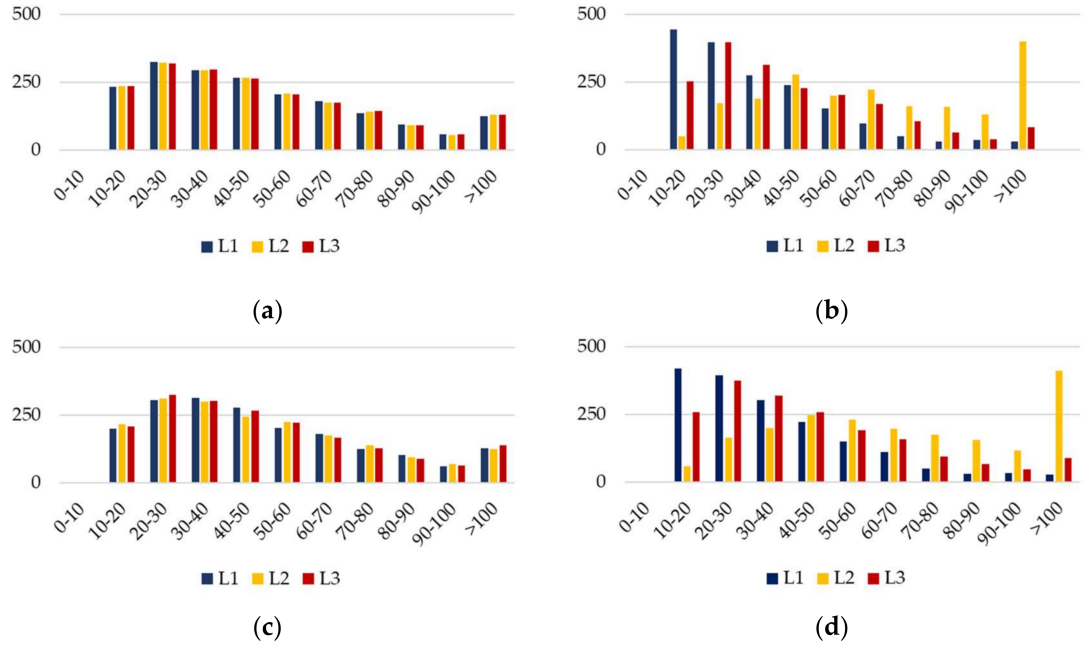

Figure 22. The number of hours during the year in which the reverse power flow is within the defined ranges (% of the rated current of transformer): (**a**) V3, (**b**) V5, (**c**) V8, and (**d**) V10.

Table 10 shows the risk of energy losses increasing in the CIGRE test network with connected PV sources. To calculate the risk, the energy losses in V2–V5 variants were

compared to losses in the V1 variant, while losses in V7–V10 variants were compared to losses in the V6 variant. For all variants with PV sources, an increase in energy losses is observed. The risk of increasing losses is much higher in variants where the penetration level of PV sources is 50%. The asymmetrical division of the PV-rated power between individual phases has a noticeable impact on the risk of increasing losses. Figure 23 shows the number of hours during the year in which the increase in energy losses is within the given ranges for variants V3, V5, V8, and V10.

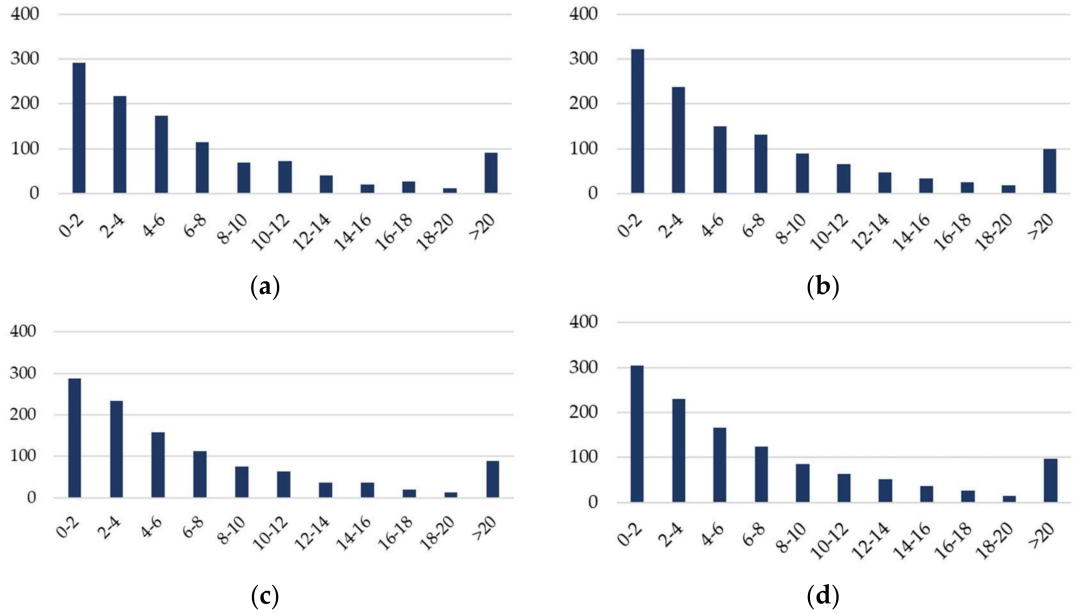

Figure 23. The number of hours during the year in which the increase in energy losses is within the defined ranges (kWh): (a) V3, (b) V5, (c) V8, and (d) V10.

4. Discussion

When comparing the daily variability of phase-to-phase load bus voltages (Figure 12, Figure 14, and Figure 16, and the corresponding figures in Appendix A), the voltage increases are particularly noticeable during periods in which PV power generation exceeds the power demand. The greater the installed capacity of PV micro-installations, the greater the voltage increases. For variants where the PV penetration level is 50%, the differences between the minimum and maximum voltages in certain buses (e.g., bus R15) reach 90 V. The minimum voltage occurs at approximately 9 p.m., coinciding with high customer demand and no PV generation. The maximum voltage occurs at approximately noon, coinciding with low customer demand and high PV generation. In these circumstances, overvoltage can occur, which may cause damage to the receivers powered from the bus. To avoid exceeding the upper limit of the bus voltage, inverters are equipped with overvoltage protections, which cause them to automatically deactivate. Deactivating PV installations is unfavorable to their owners due to the interruption of energy production, independent of the weather conditions. The results show that within the CIGRE test network, the risk of the bus voltages going beyond the relevant bounds is substantial within only certain buses when using variants where the PV penetration level is 50%. The risk did not exceed 0.8%, meaning that bus voltages were outside the permissible values for no more than 70 h during the year.

The operation of PV micro-installations has a two-fold impact on the flow of currents within the network (Figures A13, A15 and A17, and the corresponding figures in Appendix A). When PV generation is lower than demand, the load of network elements is reduced without the current direction changing. This is a favorable situation and, among other effects, provides a reduction in transmission losses. Correspondingly, during periods

in which PV generation exceeds demand, a change in the direction of current flow occurs: Power flows in reverse, from the LV network to the MV network.

This reverse flow takes different values depending on the PV penetration level in the LV network. For example, on the day of the highest intensity of solar irradiance during the year (17 May), for a PV penetration level of 25%, the reverse flow within the transformer was comparable to the current flow during the evening peak of the network load (Figure 15). For a PV penetration level of 50%, the reverse flow was almost twice as high (Figure 17). The risk of incurring a reverse power flow depends on the rated power of the PV sources. For a PV penetration level of 25%, the risk of reverse power flow within the test network was approximately 14% when using variants V2 and V7. Hence, for more than 1200 h during the year (approximately 50 days), power flowed from the LV network to the MV network. For a PV penetration level of 50%, the risk increases to approximately 22% (variants V3 and V8), corresponding to almost 2000 h (more than 80 days).

The operation of the PV sources connected to the LV network also affects the load of individual components within the network. The simulations show that the MV/LV transformer was the network component most exposed to the risk of overload. The risk of overload appeared at a PV penetration level equal to 50%. With a symmetric division of the rated power of PV sources between individual phases (variants V3 and V8), the risk of overload was approximately the same for each phase: approximately 1.5% (130 h) for the V3 variant and approximately 2.2% (190 h) for the V8 variant. The difference in risk (approximately 0.7%) is caused by the risk of overloads resulting from the asymmetry of the load (variant V6). With the asymmetric division of the power of PV sources between individual phases (variants V5 and V10), the highest risk was observed for the maximum-loaded phase. This risk was approximately 5%, corresponding to 440 h during the year (more than 18 days). Furthermore, the overload value is notable, reaching greater than 100% of the rated current (Figure 21). In the remaining phases, both the risk and the level of overload were significantly lower. Therefore, to minimize both the risk and the degree of overload of individual network components, single-phase PV sources should be connected so that the load of individual phases is even.

The change in current flow resulting from the operation of PV sources causes a change in transmission losses (Figures 19 and A19). The yearly simulations show that the risk of increasing transmission losses occurs for all variants with modeled PV sources. For variants with a PV penetration level of 25%, the risk of increasing transmission losses ranged from 1.6% to 2.2%. However, in variants with a 50% share of PV sources, the risk ranged from 12.8% to 13.9%: doubling the rated power of PV sources resulted in an eight-fold increase in the risk of increasing energy losses. From the perspective of network users, this is an adverse situation, as it causes an increase in the variable costs of energy distribution, which translates into an increase in the rates of distribution charges.

Voltage asymmetry is a common occurrence within the LV network. In addition to impedance asymmetry, voltage unbalance is primarily caused by the uneven load of individual phases due to the operation of single-phase receivers. PV sources can also be deployed as single-phase installations, and with an uneven distribution of their power between individual phases, they can affect the level of voltage unbalance. This phenomenon is visible when comparing Figures 18, A15, A17 and A18: voltage unbalance increases (the negative sequence component of the bus voltage increases) due to the operation of PV sources with power distributed asymmetrically between individual phases. However, it should be emphasized that the yearly simulations show that the limiting value of the negative sequence component of the bus voltage was not exceeded as a result of the operation of the PV sources. Moreover, the operation of PV sources did not reduce the nodal voltage below the permissible values.

Comparing the results obtained by us with those described in similar studies, one can notice their general consistency. The authors of the article [7] concluded that overload of network components and overvoltage appears only with high PV penetration levels. In addition, in our simulations, overload of network components and overvoltage appeared

at the 50% PV penetration level. The same article also shows a very strong relationship between reverse power flow and the PV penetration level. Our research also confirms this relationship. Articles [8–10] emphasize that PV sources reduce total losses until a certain penetration level and further increase in PV installations also increases grid losses. Our research also confirmed this observation. The article [11] states that the influence of PV sources on voltage asymmetry is at the level of 1%. In our research, we obtained a slightly higher value, but the level of asymmetry did not exceed the acceptable limit.

5. Conclusions

During the majority of the year, the cooperation of PV micro-installations with the power network causes no interruptions, and the parameters that characterize the operation of the LV network are within acceptable limits. Due to the growing number of prosumer micro-installations, such parameters are exceeded more frequently. The method we presented in this article determines the risk of exceeding the normal operating conditions of an LV network due to the operation of connected PV sources. Hence, the method can be used to determine the HC of existing LV networks at which the assumed risk of exceeding the individual parameters that characterize the operation of the network will be met. This method can also be used to assess the impact of newly connected PV micro-installations on the operation of the existing LV network.

As part of further research, we plan to develop a method that allows the connection of a greater number of PV micro-installations without the need for substantial development of the network. This will be achieved by increasing energy consumption at the place of its production during generation. That is, by increasing the self-consumption of the energy produced by prosumers. Selected receivers and electric energy storage devices owned by prosumers can be used for this purpose. Energy storage devices connected to the MV/LV substation that powers the given network can also be used to increase the hosting capacity of the network. The development of a method to optimally control selected receivers and energy storage devices will allow the hosting capacity of existing LV networks to be increased while maintaining the assumed risk level of exceeding the normal operating conditions. This method could also be used to control the LV network. The application of the method should make the operation of the LV grid more flexible, which is necessary for the development of electromobility, among other purposes [33].

Author Contributions: Conceptualization, R.K.; methodology, R.K., M.P. and M.S.; validation, R.K., M.P. and M.S.; formal analysis, R.K., M.P. and M.S.; investigation, R.K., M.P., and M.S.; resources, R.K., M.P. and M.S.; data curation, R.K., M.P. and M.S.; writing—original draft preparation, R.K. and M.P.; writing—review and editing, R.K., M.P. and M.S.; visualization, M.S. and R.K.; supervision, R.K. All authors have read and agreed to the published version of the manuscript.

Funding: This research received no external funding.

Data Availability Statement: Data available on demand.

Conflicts of Interest: The authors declare no conflict of interest.

Appendix A

Daily simulation results for variants V4–V10, showing phase-to-phase voltages, phase currents, negative sequence components of bus voltage, and energy losses.

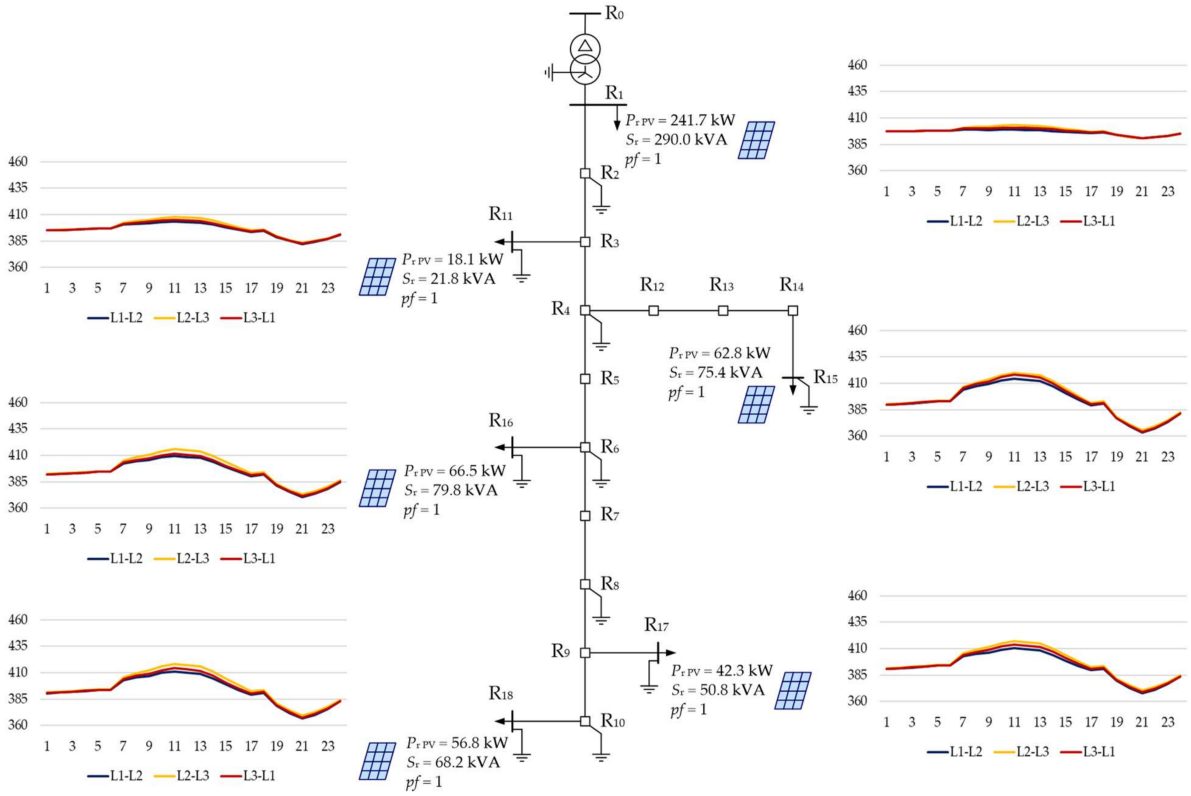

Figure A1. Daily simulation results for variant V4: phase-to-phase voltages (V).

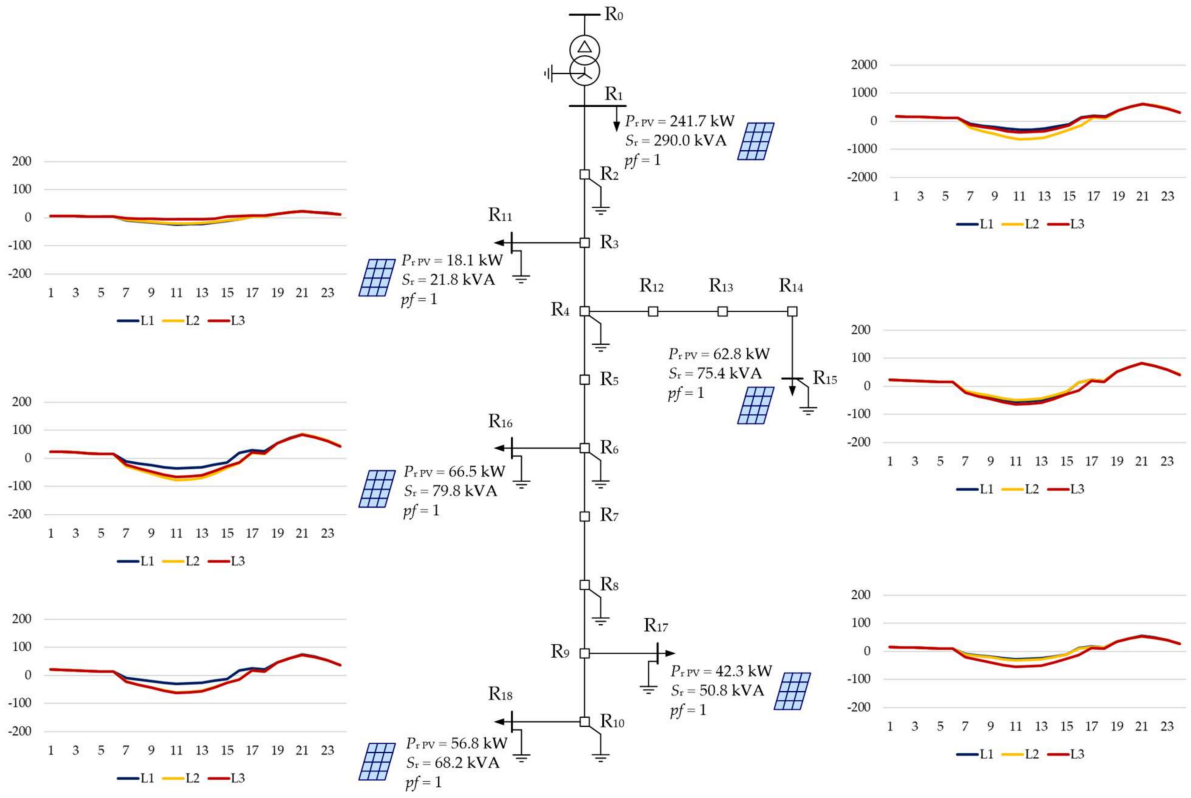

Figure A2. Daily simulation results for variant V4: phase currents (A).

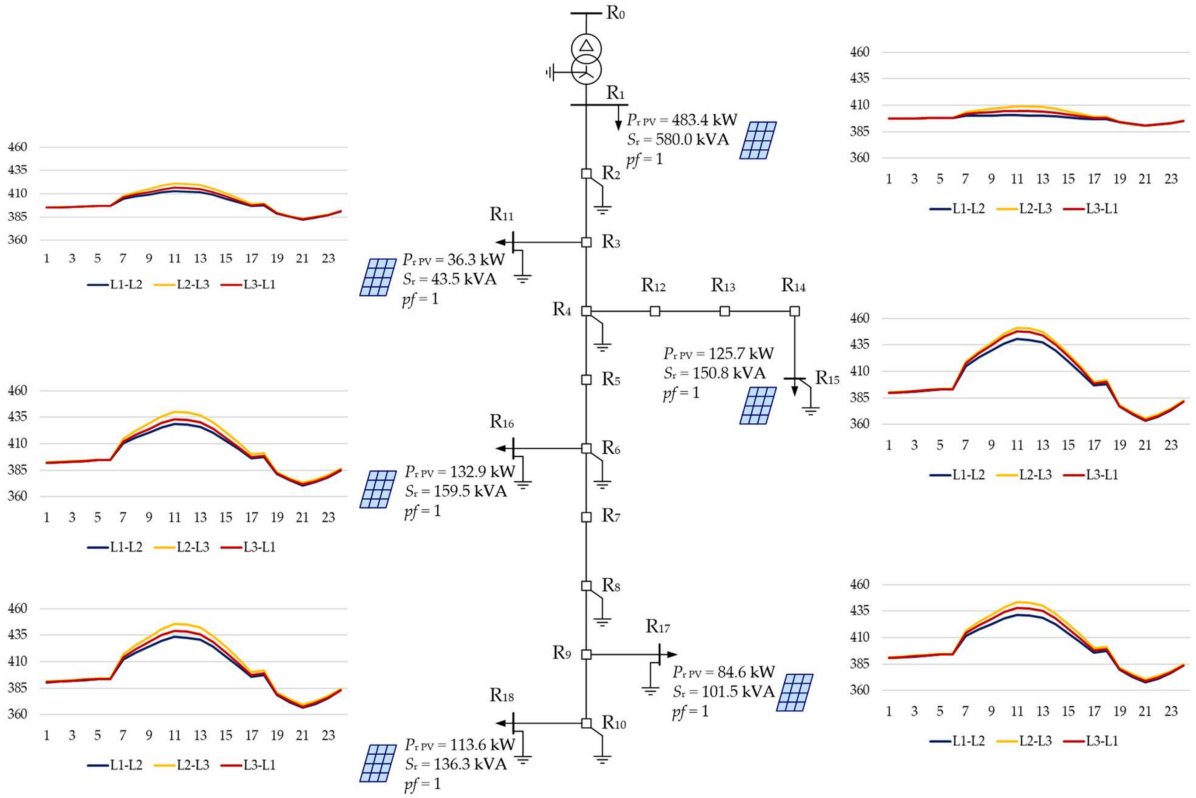

Figure A3. Daily simulation results for variant V5: phase-to-phase voltages (V).

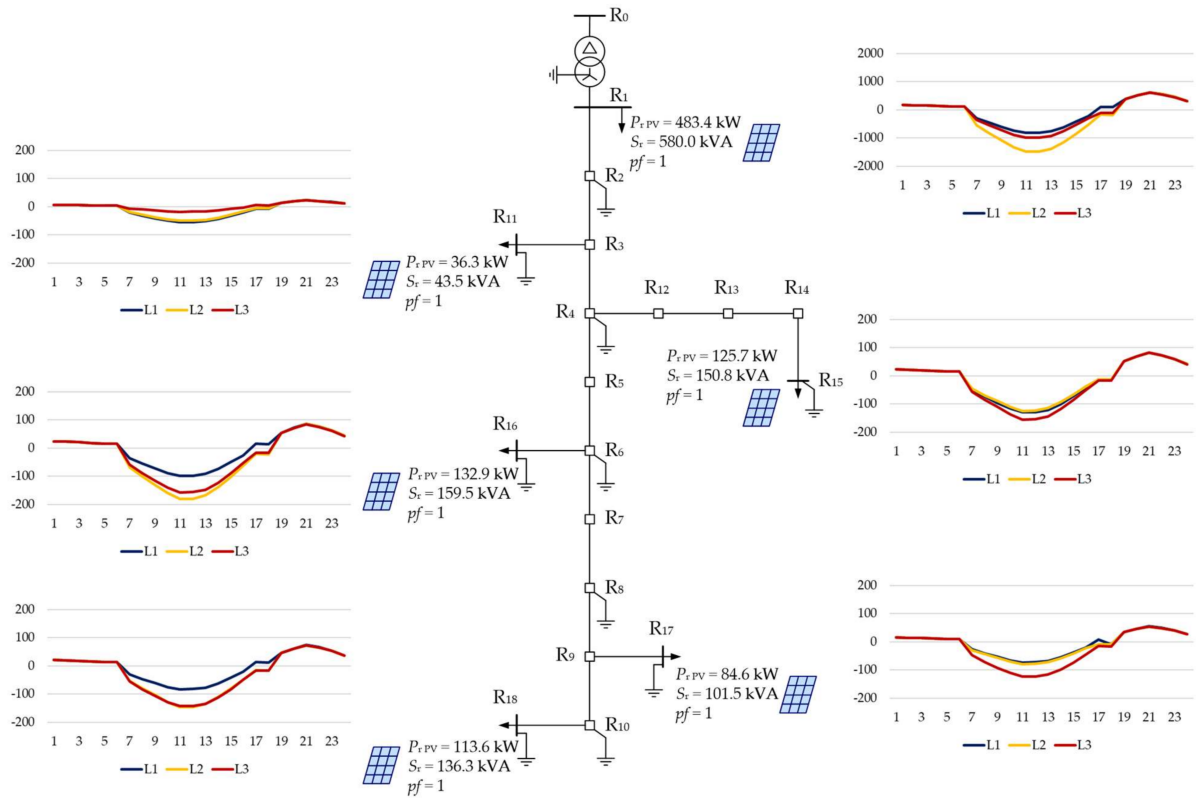

Figure A4. Daily simulation results for variant V5: phase currents (A).

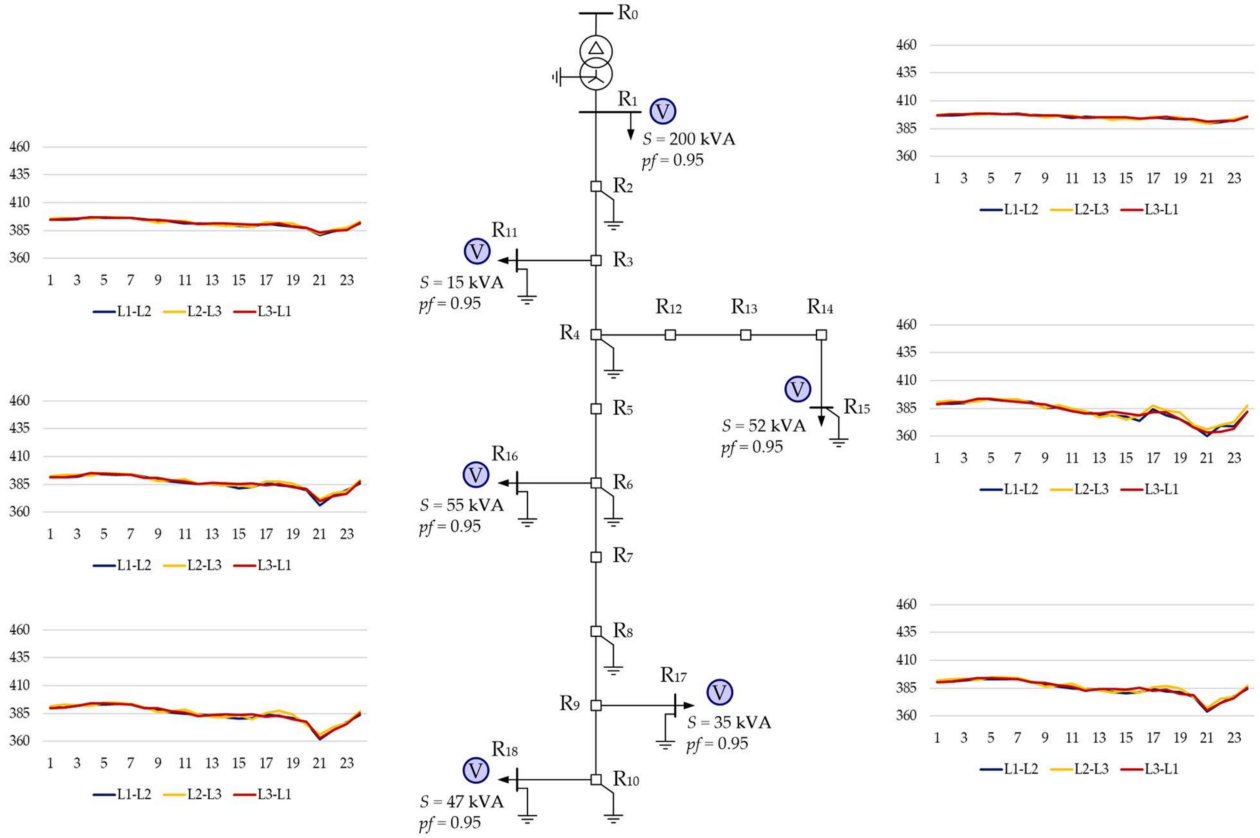

Figure A5. Daily simulation results for variant V6: phase-to-phase voltages (V).

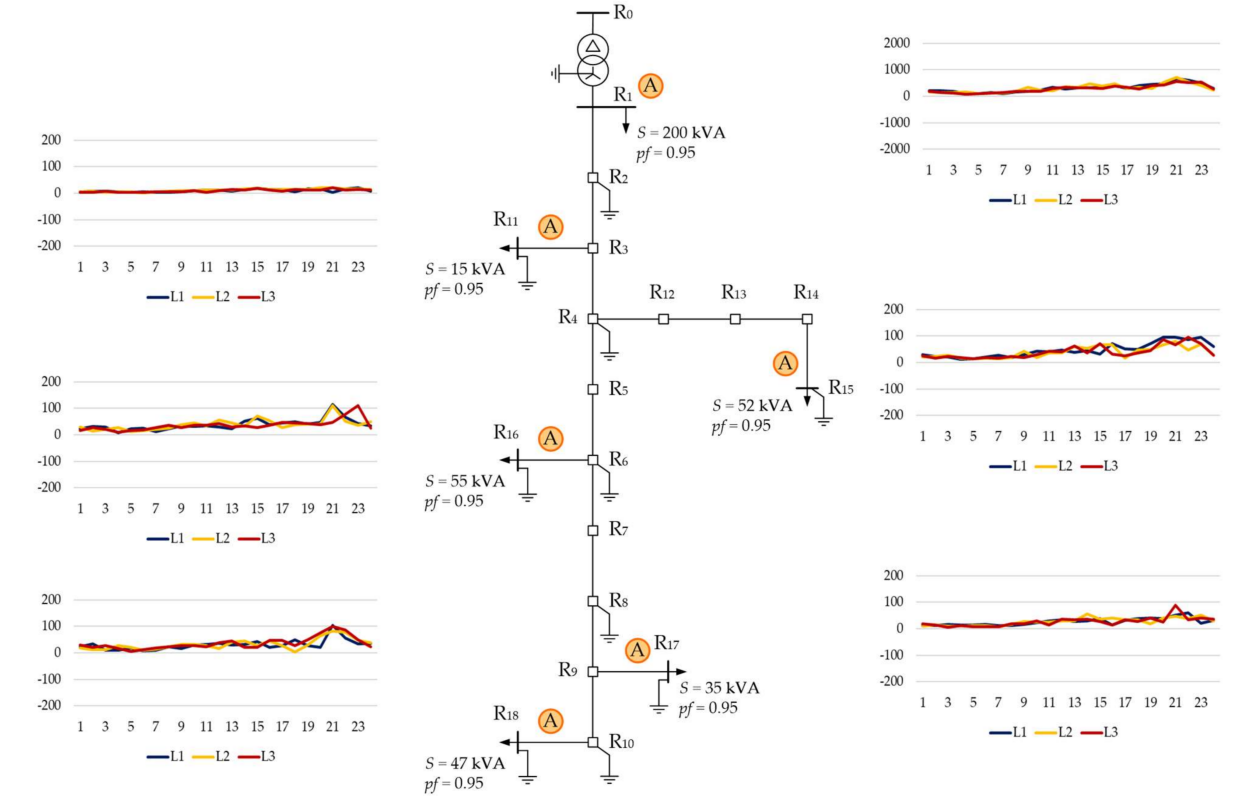

Figure A6. Daily simulation results for variant V6: phase currents (A).

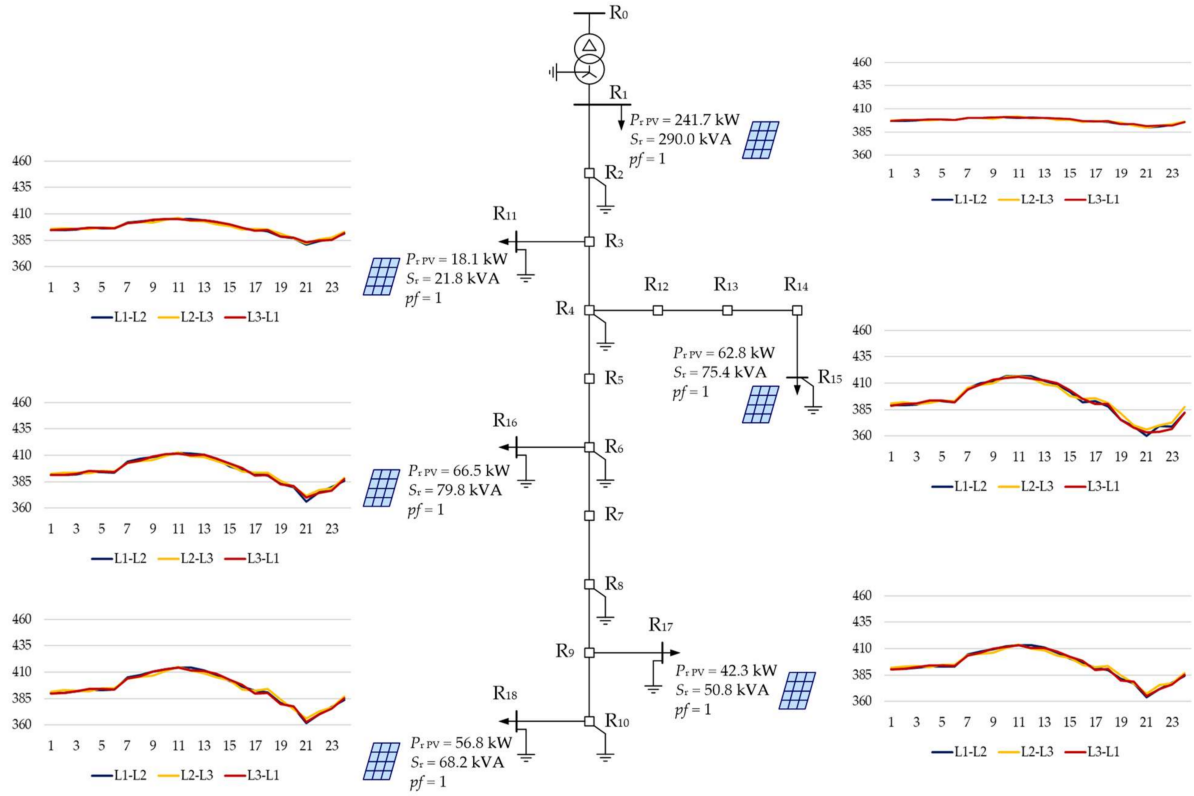

Figure A7. Daily simulation results for variant V7: phase-to-phase voltages (V).

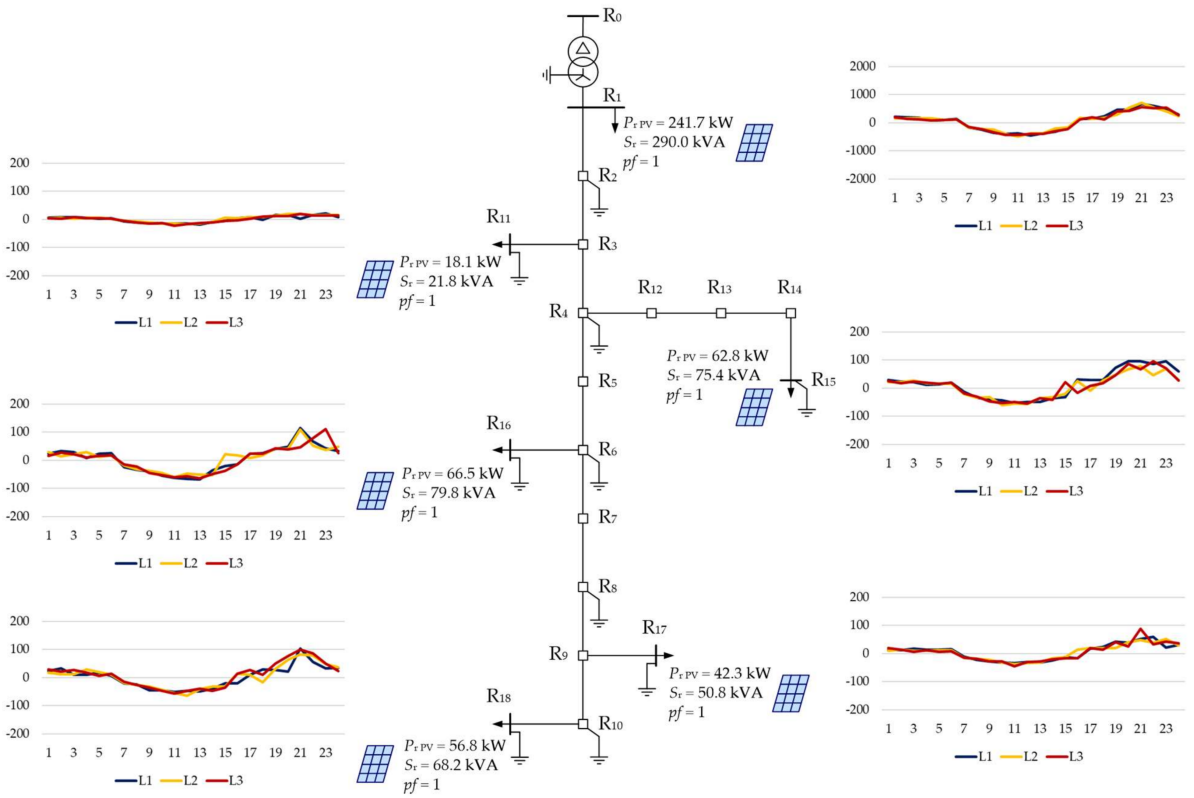

Figure A8. Daily simulation results for variant V7: phase currents (A).

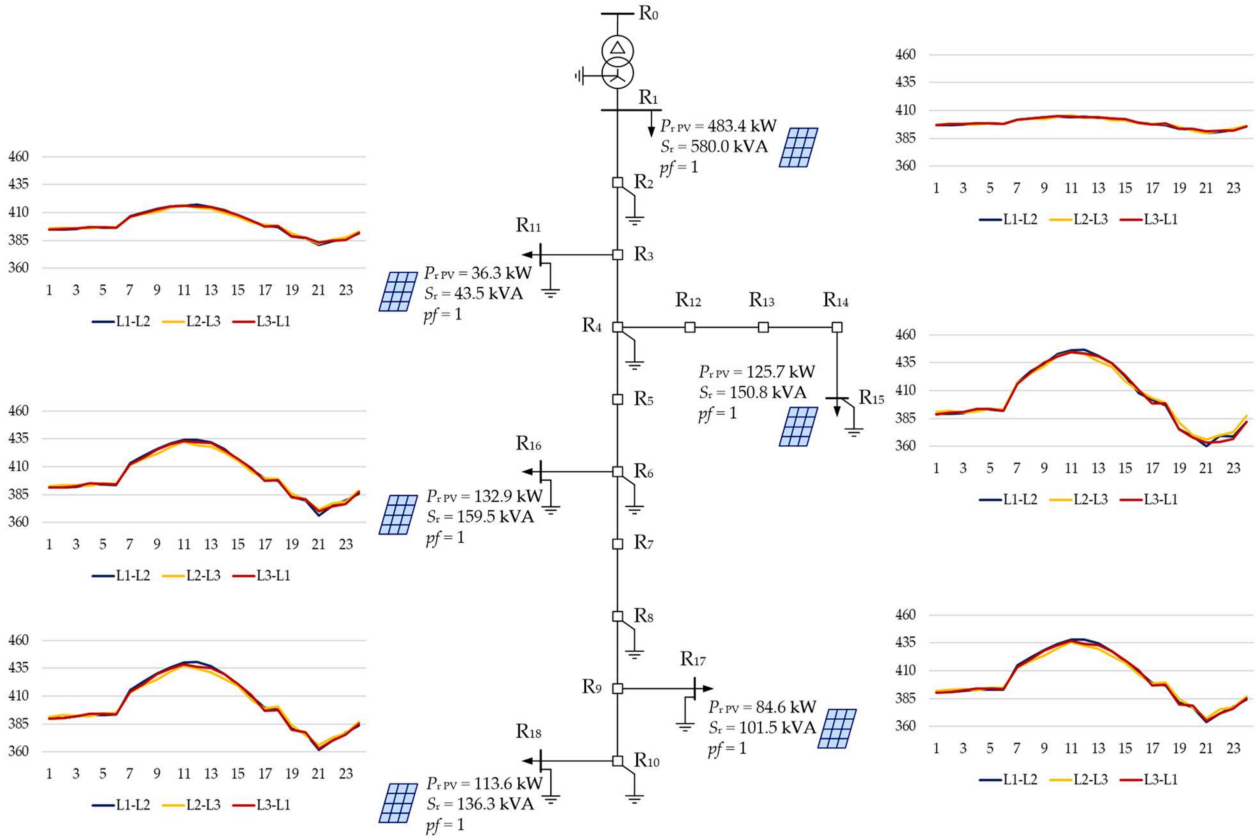

Figure A9. Daily simulation results for variant V8: phase-to-phase voltages (V).

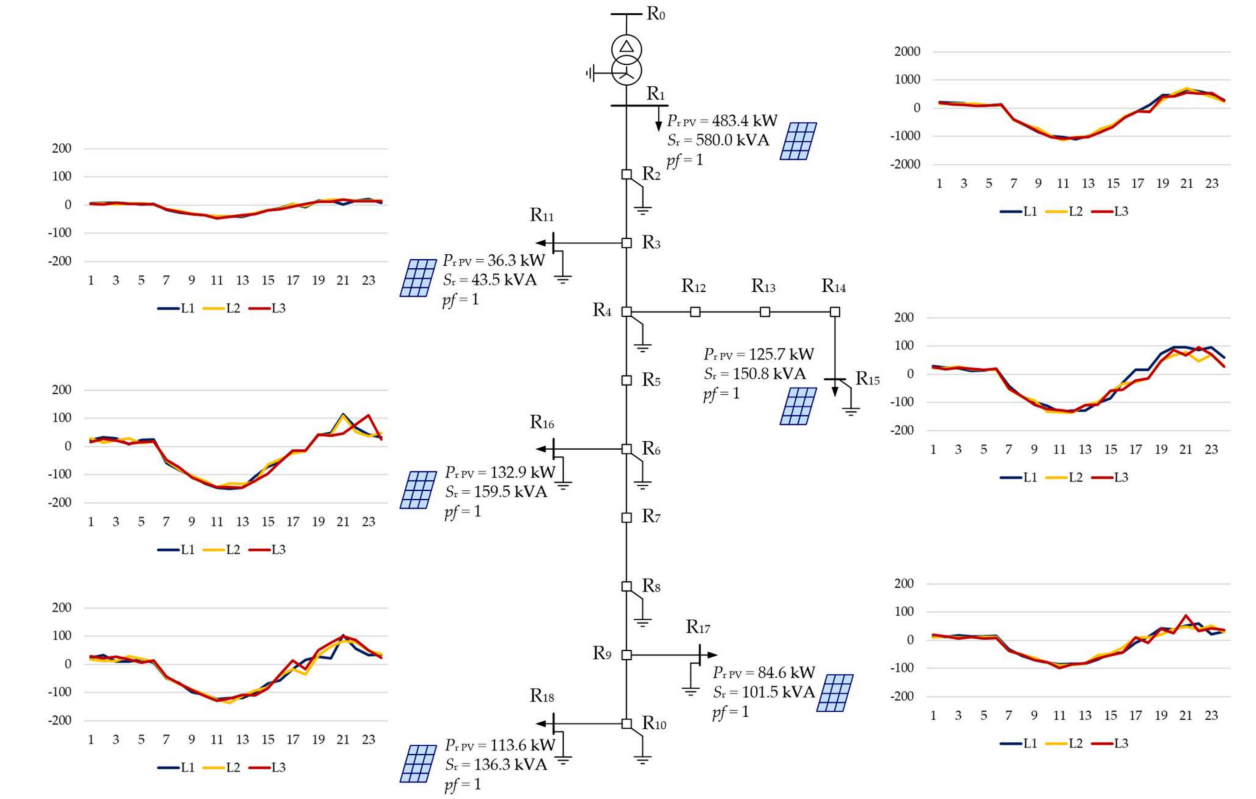

Figure A10. Daily simulation results for variant V8: phase currents (A).

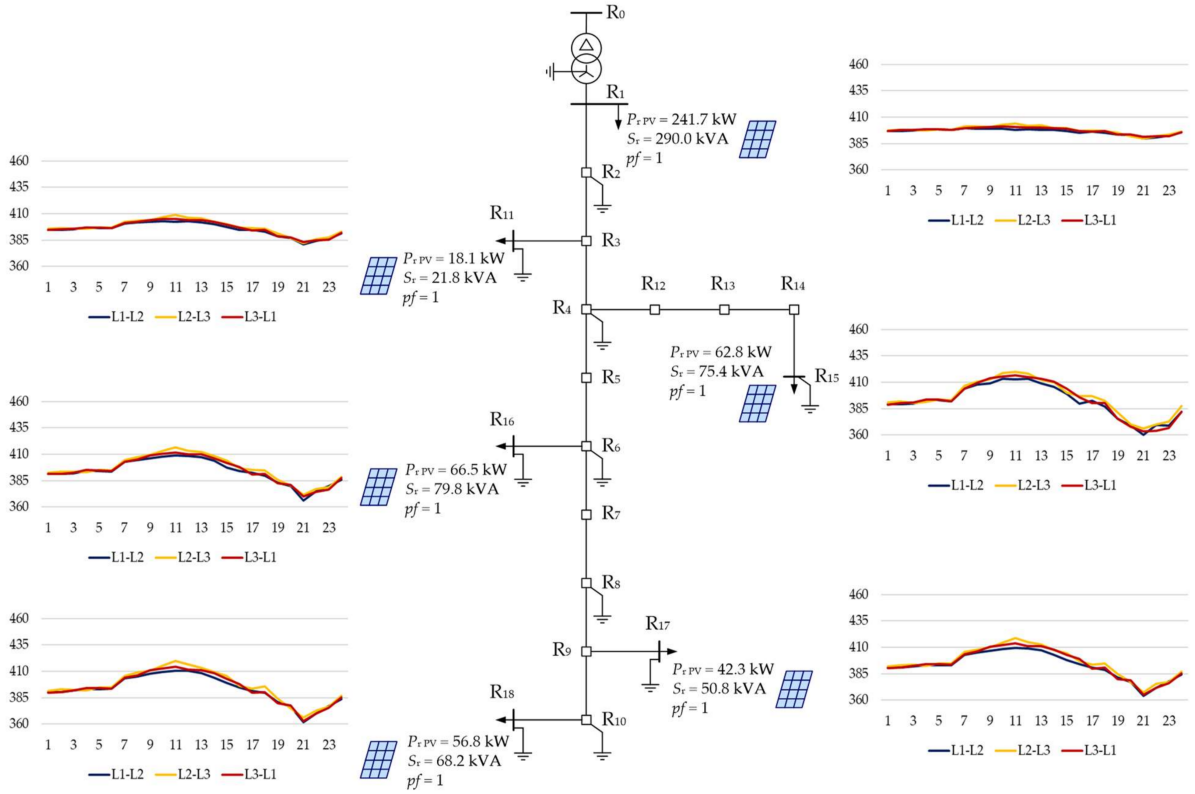

Figure A11. Daily simulation results for variant V9: phase-to-phase voltages (V).

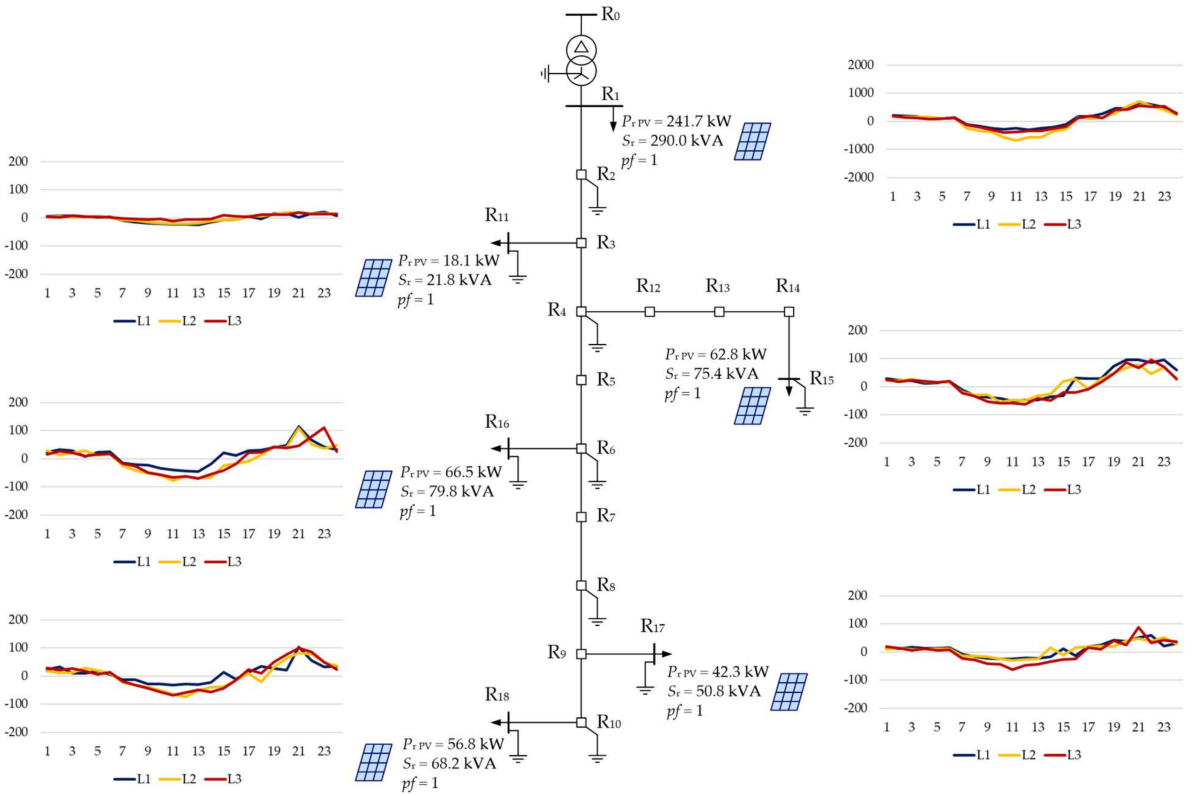

Figure A12. Daily simulation results for variant V9: phase currents (A).

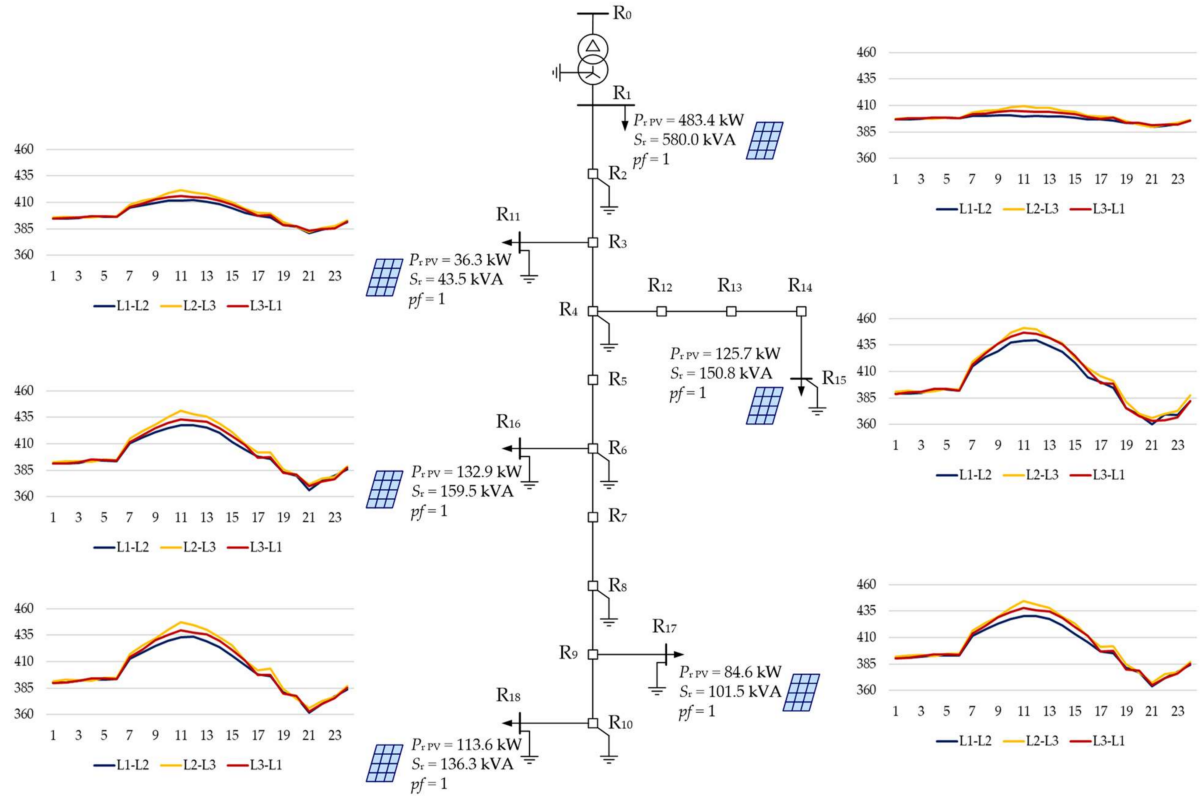

Figure A13. Daily simulation results for variant V10: phase-to-phase voltages (V).

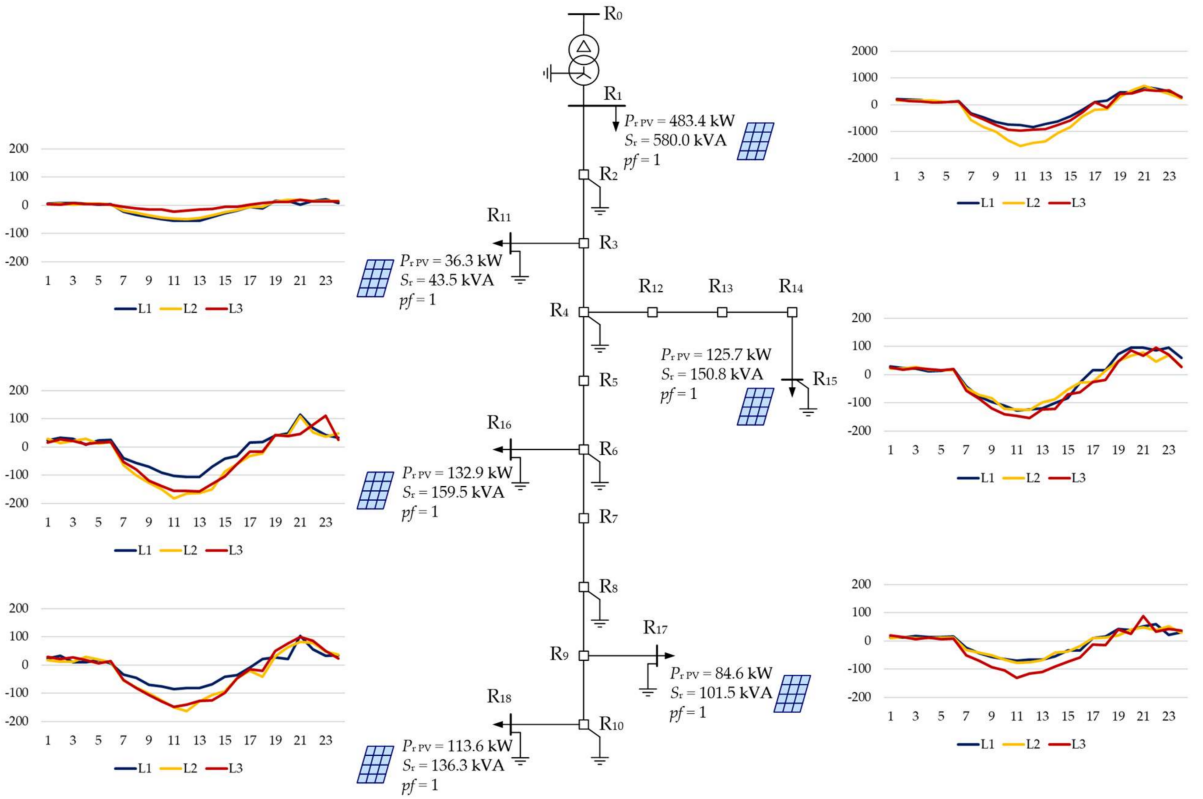

Figure A14. Daily simulation results for variant V10: phase currents (A).

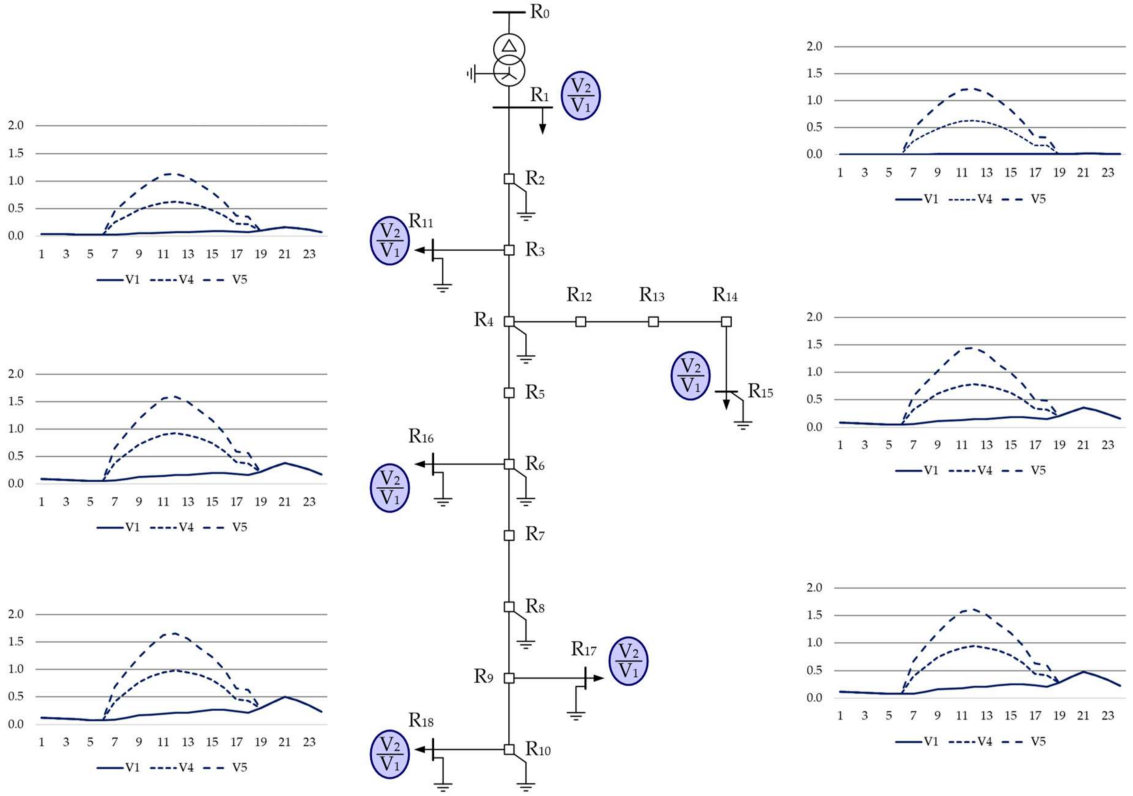

Figure A15. Daily simulation results for variants V1, V4, and V5: negative sequence component of bus voltage (%).

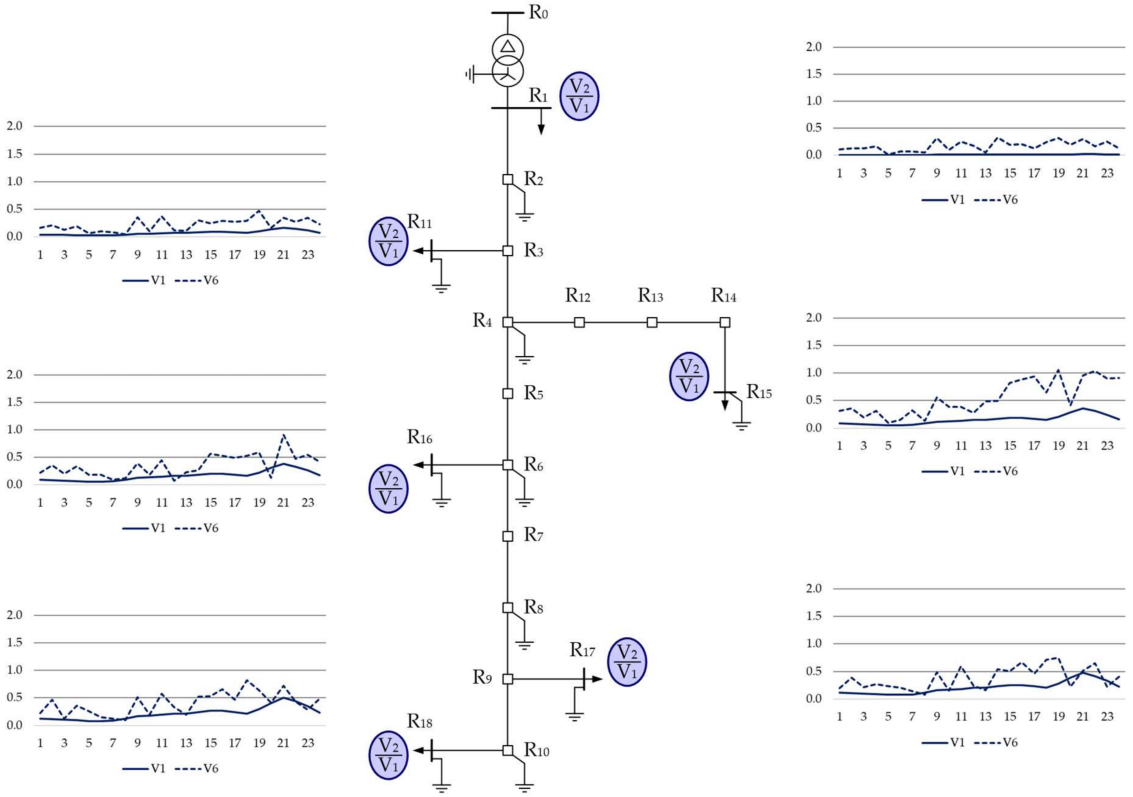

Figure A16. Daily simulation results for variants V1 and V6: negative sequence component of bus voltage (%).

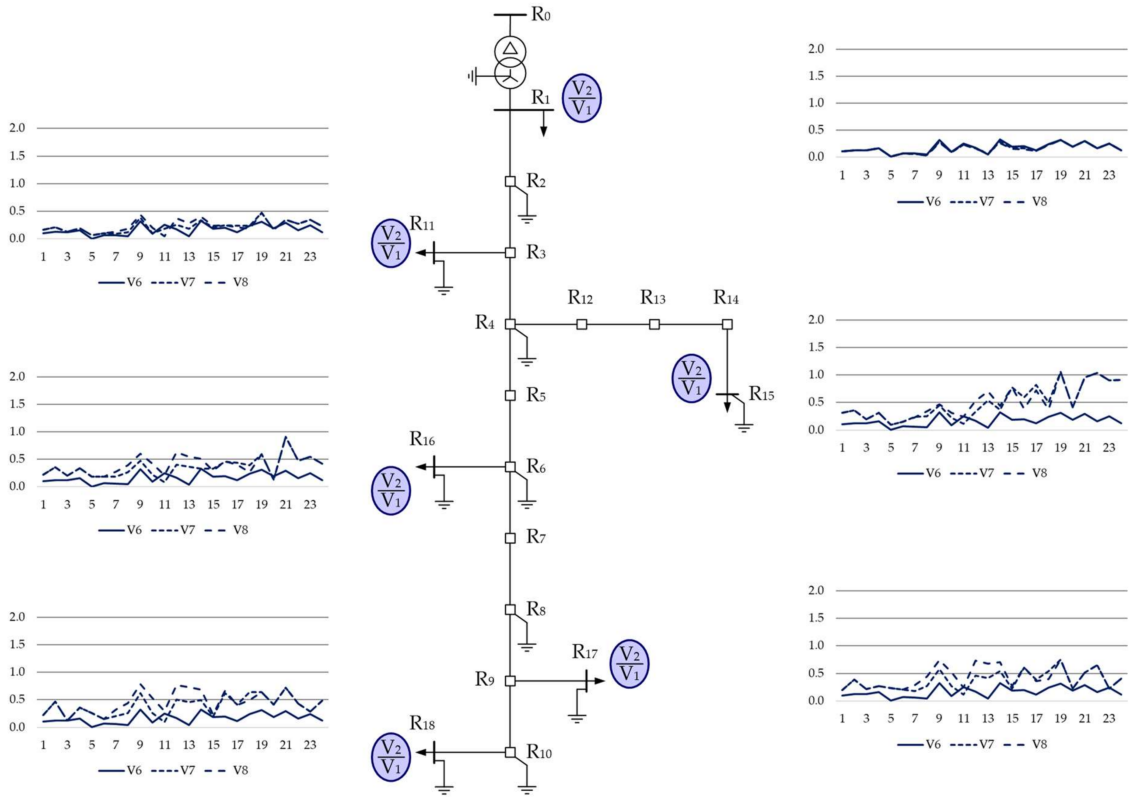

Figure A17. Daily simulation results for variants V6, V7, and V8: negative sequence component of bus voltage (%).

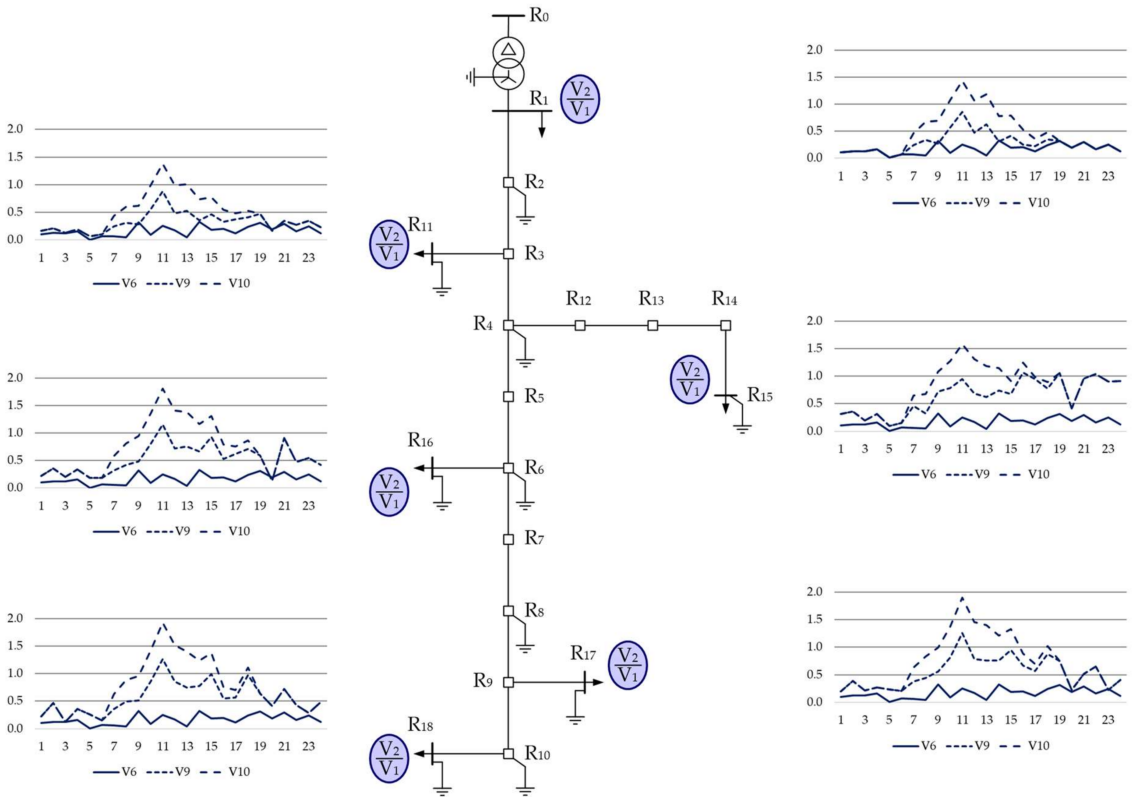

Figure A18. Daily simulation results for variants V6, V9, and V10: negative sequence component of bus voltage (%).

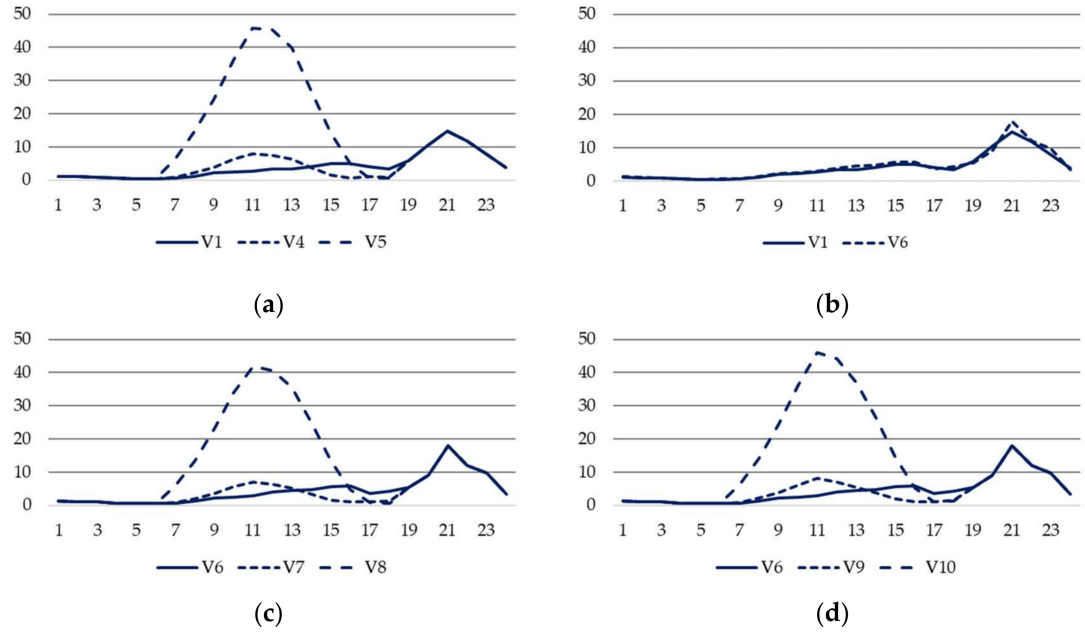

Figure A19. Daily simulation results for variants (a) V1, V4, and V5; (b) V1 and V6; (c) V6, V7, and V8; and (d) V6, V9, and V10: energy losses (kWh).

References

1. International Renewable Energy Agency. Renewable Energy Technologies. Available online: https://www.irena.org/Statistics/View-Data-by-Topic/Capacity-and-Generation/Technologies (accessed on 9 September 2021).
2. Institute for Renewable Energy. Photovoltaics in Poland 2020 summary by IEO. Available online: https://ieo.pl/en (accessed on 9 September 2021).
3. Polish Power Transmission and Distribution Association. Microinstallations in Poland. Available online: http://www.ptpiree.pl/energetyka-w-polsce/energetyka-w-liczbach/mikroinstalacje-w-polsce (accessed on 9 September 2021). (In Polish).
4. Olczak, P.; Kryzia, D.; Matuszewska, D.; Kuta, M. "My Electricity" Program Effectiveness Supporting the Development of PV Installation in Poland. *Energies* **2021**, *14*, 231. [CrossRef]
5. Legal Sources on Renewable Energy. Support Scheme for Prosumers. Available online: http://www.res-legal.eu/en/search-by-country/poland/single/s/res-e/t/promotion/aid/support-scheme-for-prosumers-1/lastp/175/ (accessed on 9 September 2021).
6. Wójcicki, R. Solar photovoltaic self-consumption in the Polish prosumer sector. *Rynek Energii* **2020**, *1*, 11–17. (In Polish)
7. Watson, J.D.; Watson, N.R.; Santos-Martin, D.; Wood, A.R.; Lemon, S.; Miller, A.J. Impact of solar photovoltaics on the low-voltage distribution network in New Zealand. *IET Gener. Transm. Distrib.* **2016**, *10*, 1–9. [CrossRef]
8. Singh, R.; Tripathi, P.; Yatendra, K. Impact of Solar Photovoltaic Penetration in Distribution Network. In Proceedings of the 2019 3rd International Conference on Recent Developments in Control, Automation & Power Engineering (RDCAPE), Noida, India, 10–11 October 2019.
9. Alboaouh, K.A.; Mohagheghi, S. Impact of Rooftop Photovoltaics on the Distribution System. *J. Renewable Energy* **2020**, *2020*, 4831434. [CrossRef]
10. Fernández, G.; Galan, N.; Marquina, D.; Martínez, D.; Sanchez, A.; López, P.; Bludszuweit, H.; Rueda, J. Photovoltaic Generation Impact Analysis in Low Voltage Distribution Grids. *Energies* **2020**, *13*, 4347. [CrossRef]
11. Gandhi, O.; Kumar, D.S.; Rodríguez-Gallegos, C.D.; Srinivasan, D. Review of power system impacts at high PV penetration. Part I: Factors limiting PV penetration. *Solar Energy* **2020**, *210*, 181–201. [CrossRef]
12. Uzum, B.; Onen, A.; Hasanien, H.M.; Muyeen, S.M. Rooftop Solar PV Penetration Impacts on Distribution Network and Further Growth Factors—A Comprehensive Review. *Electronics* **2021**, *10*, 55. [CrossRef]
13. Ismael, S.M.; Shady, H.E.; Aleem, A.; Abdelaziz, A.Y.; Zobaa, A.F. State-of-the-art of hosting capacity in modern power systems with distributed generation. *Renew. Energy* **2019**, *130*, 1002–1020. [CrossRef]
14. Mulenga, E.; Bollen, M.H.J.; Etherden, N. A review of hosting capacity quantification methods for photovoltaics in low-voltage distribution grids. *Int. J. Electr. Power Energy Syst.* **2020**, *115*, 105445. [CrossRef]
15. Zain ul Abideen, M.; Ellabban, O.; Al-Fagih, L. A Review of the Tools and Methods for Distribution Networks' Hosting Capacity Calculation. *Energies* **2020**, *13*, 2758. [CrossRef]
16. Fatima, S.; Püvi, V.; Lehtonen, M. Review on the PV Hosting Capacity in Distribution Networks. *Energies* **2020**, *13*, 4756. [CrossRef]

17. Bollen, M.H.J.; Rönnberg, S.K. Hosting Capacity of the Power Grid for Renewable Electricity Production and New Large Consumption Equipment. *Energies* **2017**, *10*, 1325. [CrossRef]
18. Wang, X.F.; Song, Y.; Irving, M. *Modern Power Systems Analysis*; Springer: New York, NY, USA, 2008.
19. Gong, Q.; Lei, J.; Qiao, H.; Qiu, J. Risk Assessment for Distribution Systems Using an Improved PEM-Based Method Considering Wind and Photovoltaic Power Distribution. *Sustainability* **2017**, *9*, 491. [CrossRef]
20. Ji, S.; Wang, Q.; Ding, N.; Liang, L. Analysis and Assessment of Operation Risk for Power System with Photovoltaic Power Stations. In Proceedings of the 2018 5th International Conference on Electric Power and Energy Conversion Systems (EPECS), Kitakyushu, Japan, 23–25 April 2018; pp. 1–6. [CrossRef]
21. Pukhrem, S.; Basu, M.; Conlon, M.F. Probabilistic Risk Assessment of Power Quality Variations and Events Under Temporal and Spatial Characteristic of Increased PV Integration in Low-Voltage Distribution Networks. *IEEE Trans. Power Syst.* **2018**, *33*, 3246–3254. [CrossRef]
22. Tao, S.; Li, C.; Zhang, L.; Tang, Y. Operational Risk Assessment of Grid-connected PV System Considering Weather Variability and Component Availability. *Energy Procedia* **2018**, *145*, 252–258. [CrossRef]
23. Wang, L.; Yuan, M.; Zhang, F.; Wang, X.; Dai, L.; Zhao, F. Risk Assessment of Distribution Networks Integrating Large-Scale Distributed Photovoltaics. *IEEE Access* **2019**, *7*, 59653–59664. [CrossRef]
24. Lei, J.; Gong, Q.; Gao, D.W.; Wang, B.; Guan, X. Operation risk assessment of active distribution networks considering probabilistic uncertainties of distributed generators-loads and power management of VRB ESSs. *IET Renew. Power Gener.* **2020**, *14*, 1764–1771. [CrossRef]
25. CIGRE Technical Brochure. Benchmark Systems for Network Integration of Renewable and Distributed Energy Resources. Task Force C6.06. 2014. Available online: http://e-cigre.org/publication/575-benchmark-systems-for-network-integration-of-renewable-and-distributed-energy-resources (accessed on 1 October 2020).
26. EPRI. OpenDSS. Available online: https://www.epri.com/pages/sa/opendss (accessed on 25 September 2021).
27. Wajahat, M.; Khalid, H.A.; Bhutto, G.M.; Leth Bak, C. A Comparative Study into Enhancing the PV Penetration Limit of a LV CIGRE Residential Network with Distributed Grid-Tied Single-Phase PV Systems. *Energies* **2019**, *12*, 2964. [CrossRef]
28. Kurtz, S.; Whitfield, K.; Miller, D.; Joyce, J.; Wohlgemuth, J.; Kempe, M.; Dhere, N.; Bosco, N.; Zgonena, T. Evaluation of high-temperature exposure of rack mounted photovoltaic modules. In Proceedings of the 34th IEEE Photovoltaic Specialists Conference (PVSC), Philadelphia, PA, USA, 7–12 June 2009; pp. 2399–2404. [CrossRef]
29. ISO 15927-4:2005. Hygrothermal Performance of Buildings—Calculation and Presentation of Climatic Data—Part 4: Hourly Data for Assessing the Annual Energy Use for Heating and Cooling. Available online: https://www.iso.org/standard/41371.html (accessed on 9 September 2021).
30. Ministry of Investments and Development. Data for Energy Calculations of Buildings. Available online: https://www.gov.pl/web/archiwum-inwestycje-rozwoj/dane-do-obliczen-energetycznych-budynkow (accessed on 9 September 2021). (In Polish)
31. Regulation of the Minister of Economy on the Detailed Conditions for the Operation of the Power System. Available online: http://isap.sejm.gov.pl/isap.nsf/DocDetails.xsp?id=wdu20070930623 (accessed on 19 September 2021). (In Polish)
32. Power Cables and Wires. Available online: https://www.tfkable.com/katalogi-i-broszury/katalogi.html (accessed on 19 September 2021). (In Polish).
33. Szablicki, M.; Rzepka, P.; Sołtysik, M.; Czapaj, R. The idea of non-restricted use of LV networks by electricity consumers, producers, and prosumers. In Proceedings of the 14th International Scientific Conference on Forecasting in Electric Power Engineering (PE 2018), Podlesice, Poland, 26–28 September 2018.